The joint application of metaheuristic algorithm and Bayesian Statistics approach for uncertainty and stability assessment of nonlinear Magnetotelluric data

*Mukesh Mukesh, *Kuldeep Sarkar, and Upendra K. Singh

Department of Applied Geophysics, IIT(ISM) Dhanbad, Dhanbad-826 004, Jharkhand, India

* Corresponding authors: Mukesh Mukesh (mukesh4593@gmail.com) and

Kuldeep Sarkar (kuldeepsarkar39@gmail.com)

Abstract

In this paper, we have developed the Matlab code for a weighted hybrid of particle swarm optimization (PSO) and gravitational search algorithm (GSA) known as wPSOGSA, GSA, and PSO algorithms to interpret one-dimensional magnetotelluric (MT) data for some corrupted and non-corrupted synthetic data, as well as two examples of MT field data over different geological terrains: (i) geothermal rich area, Island of Milos, Greece, and (ii) Southern Scotland due to the occurrence of a significantly high electrical conductivity anomaly under crust and upper mantle extending from the Midland Valley across the Southern Uplands into northern England. Even though the fact that many models provide a good fit in a large predefined search space, specific models do not fit well. As a result, we used a Bayesian statistical technique to construct and assess the posterior probability density function (PDF) rather than picking the global model based on the lowest misfit error. This is proceeded by 68.27 % confidence interval for selecting a region where PDF is more prevalent to estimate the mean model which is more accurate and close to the true model. For illustration, correlation matrices show a significant relationship among layer parameters. The findings indicate, the wPSOGSA is less sensitive to model parameters and produces well, more stable and reliable results with the least uncertainty in the model that is compatible with existing borehole samples. Furthermore, the present methods resolve two additional geologically significant layers, one highly conductive (less than 1.0 Ωm) and another resistive (300.0 Ωm) over the Island of Milos, Greece, characterized by alluvium and volcanic deposits, respectively, as corroborated by borehole stratigraphy.

Keywords: Magnetotelluric; Inversion; Uncertainty; wPSOGSA; Posterior; Bayesian.

1.0 Introduction

The magnetotelluric (MT) method is a natural source electromagnetic method that explores various natural resources, namely hydrocarbon, minerals, geothermal prospects, groundwater, metalliferous ores, etc. (Nabighian and Asten, 2002; Simpson and Bahr, 2005). Due to its instability, non-unique solution, and algorithm sensitivity, the MT data interpretation is thought-provoking. Many researchers have attempted and developed various inversion algorithms to interpret, improve the model accuracy, convergence speed, stability and reduce the uncertainty of the solutions (Kirkpatrick, et al., 1983; Constable et al., 1987; Rodi and Mackie, 2001; Li et al., 2018; Zhang et al., 2019; Khishe and Mosavi, 2020). There are mainly two categories of the inversion algorithm: first, the local optimization methods namely Conjugate gradient, Levenberg-Marquardt/Ridge regression, Newton-Gauss, Steepest descent, and Occam inversion, requires good initial guess (Shaw and Srivastava, 2007; Wen et al., 2019; Roy and Kumar, 2021) and another is global optimization techniques (i.e., Ant colony optimization, Genetic algorithm, Particle swarm optimization, Gravitational search algorithm, Simulated annealing, etc.) does not require initial guess. Many researchers have carried out numerous metaheuristic optimization algorithms to invert MT data (Dosso and Oldenburg, 1991; Pérez-Flores and Schultz, 2002; Miecznik et al., 2003; Sen and Stoffa, 2013). These algorithms are inspired by the natural phenomenon and have various geophysical application include Particle Swarm Optimization (Kennedy and Eberhart, 1995; Essa et al., 2023), Genetic Algorithm (Whitley, 1994), Bat algorithm (Yang, 2010a; Essa and Diab, 2023), Differential Evolution (Storn and Price, 1997), biogeographically based Optimization (Simon, 2008), Firefly algorithm (Yang, 2010b), Grey Wolves Optimizer (Mirjalili et al., 2014), Ant Colony (Colorni et al., 1991), Gravitational Search Algorithm (Rashedi et al., 2009) and novel barnacles mating optimization algorithm (Ai et al., 2022).

However, unique characteristics, namely exploration and exploitation, persist in any global optimization algorithms. For example, the PSO algorithm has a very high potential for exploitation, which implies that the algorithm performs well in local search but is inferior in exploration (Şenel et al., 2019). This suggests that the algorithm has a limited capacity to estimate the best model in an extensive search range. Because of low exploration characteristics, it gets trapped at the local minima (Mirjalili and Hashim, 2010). So, integrating the two algorithms with opposite characteristics is the best way to balance exploration and exploitation characteristics to achieve better solutions than the results obtained from an individual algorithm.

Here, we utilized wPSOGSA, a new global optimization method that takes into account the algorithm based on natural behavior seen in birds, fish, and insects known as Particle swarm optimization (PSO) and gravity-based Newton's law (with high exploration capability) known as Gravity search algorithm (GSA). Researchers interested in artificial intelligence and developing effective optimization algorithms for comparative analysis of different metaheuristic algorithms (Pace et al., 2022) have been drawn to notable characteristics in such social behavior. The wPSOGSA, PSO, and GSA are used to estimate resistivity distribution of 1D multi-layered earth model using synthetic (noise free and noisy) data for three and four layers cases taken from (Shaw and Srivastava, 2007)) and Xiong et al. (2018), respectively and field MT sounding data for six and four layers cases taken from (Hutton et al., 1989) and (Jones and Hutton, 1979) respectively.F

Furthermore, numerous (here 10000) models that fit well are optimized for getting the mean model, which is proceeded by calculating posterior PDF based on Bayesian concepts using all accepted models to find the optimal mean solution with the least uncertainty, as well as a correlation matrix to determine the relationships among the layer parameters. Thus, the research reveals that the wPSOGSA method may be utilized to provide a more accurate and reliable model with superior stability, a quick rate of convergence, and the least amount of model uncertainty.

2.0 Data and Methodology

2.1 Synthetic and field data

Different MT datasets are utilized to evaluate the proposed wPSOGSA algorithm's effectiveness, sensitivity, stability, and robustness in outlining the genuine subsurface structure. These datasets are noise-free and Gaussian noise synthetic data produced for several geological formations, and two MT field data have been optimized for analysis.

To demonstrate and evaluate the robustness of the present algorithms, we have generated a synthetic MT apparent resistivity and apparent phase data without noise and with noise levels (10 % and 20 % noise) considering a three-layer typical continental crustal model with a total thickness of 33000 m (i.e., 33.0 km) having a resistivity of upper-crust 30000.0 Ωm with 15000 m (i.e., 15 km) thickness (high resistive layer) and resistivity of middle crust 5000.0 Ωm with 18000 m (i.e., 18.0 km) thickness (reasonable low resistive layer) underlain by 1000 Ωm (low resistive) half space taken from (Shaw and Srivastava, 2007).

For the second example of the synthetic data, a typical four-layer HK-type of earth model taken from Xiong et al. (2018) is generated by forward modeling equations for the demonstration of the wPSOGSA, PSO, and GSA algorithms and compared their performance with Improved Differential Evolution (IDE) results obtained by Xiong et al. (2018).

We utilized the first example of field data taken from (Hutton et al., 1989), the Island of Milos, Greece. Milos is a part of the South Aegean Active Volcanic Arc, an example of an emergent volcanic edifice (Stewart and McPhie, 2006) formed by monogenetic effusive and explosive magmatism pulses. Milos is the world's biggest exporter of bentonite, and it also has a diverse variety of metalliferous and non-metalliferous mineral reserves. It's a conserved on-land laboratory for studying shallow underwater hydrothermal ore-forming processes. The accompanying shallow subsurface hydrothermal venting fields have developed significantly less attention. In ("Dawes, 1986), used magnetotelluric data to assess the resistivity structure of the geothermal area on Milos west side. With around 3.0 km spacing, 37 MT probes in the bandwidth of 100-0.01 Hz and 12 investigations in the bandwidth of 0.01-0.0001 Hz were installed along with various profiles that were perpendicular to the Zephyria graben in the W-E direction, as well as along the graben in S-N direction (Hutton et al., 1989).

Another field example of MT data from (Jones and Hutton, 1979) was picked to illustrate our technique from Newcastleton (2.796° W, 55.196° N in Geographic coordinates), Southern Uplands of Scotland. By the Southern Uplands fault, the Southern Uplands are isolated from the Midland Valley. The bulk of the Southern Uplands comprises Silurian/Lower Paleozoic sedimentary deposits such as greywackes and shales that originated in the Iapetus Ocean during the late Neoproterozoic and early Paleozoic geologic eras. These rocks emerged from the seafloor as an accretionary wedge during the Caledonian orogeny. The majority of the rocks are coarse greywacke, a kind of sandstone that has been poorly metamorphosed and contains angular quartz, feldspar, and small rock fragments. The Midland Valley and Northern England, on the other hand, are known for their thick Carboniferous layers, which are used to measure coal.

2.2 Forward Modelling- Magnetotelluric formulation for 1-D earth

The ability to formulate an effective inversion method requires a thorough understanding of the forward modeling technique for the issue of interest. Factors like frequency range, actual resistivity, and layer thickness are used to create synthetic MT apparent resistivity, $\rho_a(\omega)$ and apparent phase, $\varphi_a(\omega)$ data sets. The electromagnetic impedance (Z) for layered structures is described in terms of an orthogonal electric field, magnetic field, wavenumber (k), reflection coefficient (R), and exponent factor (τ_f) with angular frequency (ω) as (Ward and Hohmann, 1988):

$$Z = \frac{\mu_0 \omega}{k} = \frac{E_x}{H_y} = -\frac{E_y}{H_x} \qquad (1)$$

where, the wavenumber$(k) = \sqrt{-i\mu_0 \omega / \rho}$, component of electric field (E_x and E_y) and magnetic field component (H_x and H_y).

If displacement currents are not taken into account, Eq. (1) becomes

$$Z = \frac{\mu_0 \omega}{\sqrt{-i\mu_0\omega/\rho}} = \sqrt{i\mu_0\omega\rho} = \sqrt{\mu_0\omega\rho}\, e^{\frac{i\pi}{4}} = \omega\,\frac{(1 - \mathrm{R}\,\tau_f)}{(1+ \mathrm{R}\,\tau_f)} \qquad (2)$$

Noisy impedance is calculated by the following equation

$$Z_{noisy} = Z + Z \times (2 \times rand - 1) \times noise_{percent} \qquad (3)$$

If the angle between impedance phase with E_x is 45^0, then the resistivity (ρ) in half-space of impedance $Z(\omega)$ and time period (T) can be written as

$$\rho(\omega) = \frac{1}{\mu_0\omega}\,|Z(\omega)|^2 = \frac{0.2T}{\mu_0}\left|\frac{E_x}{H_y}\right|^2 \qquad (4)$$

Thus, the apparent resistivity and apparent phase are defined (Cagniard, 1953; Ward and Hohmann, 1988) as follows:

Apparent resistivity, $\rho_a(\omega) = \frac{1}{\mu_0\omega}[Z(\omega)Z^*(\omega)]$ (5)

Apparent phase, $\varphi_a(\omega) = tan^{-1}\left(\frac{img(Z(\omega))}{real(Z(\omega))}\right)$ (6)

where, the exponent factor, $\tau_f = \exp(-2\gamma h)$, the induction parameter $\gamma = \sqrt{i\omega\mu_0/\rho}$, h is the layer thickness, μ_0 is the magnetic permeability for free space, Z^* is the complex conjugate of impedance, and the *rand* is used for generating random number between 0 and +1.

2.3 Global optimization technique

The techniques that we have used for joint modeling of metaheuristic global optimization namely PSO, GSA, and wPSOGSA in Step-1 and posterior Bayesian probability density function technique in Step-2 to obtain the global model by utilizing the synthetic data generated by using forward modelling and field MT apparent resistivity and phase curves is depicted in the schematic diagram (Fig. 1).

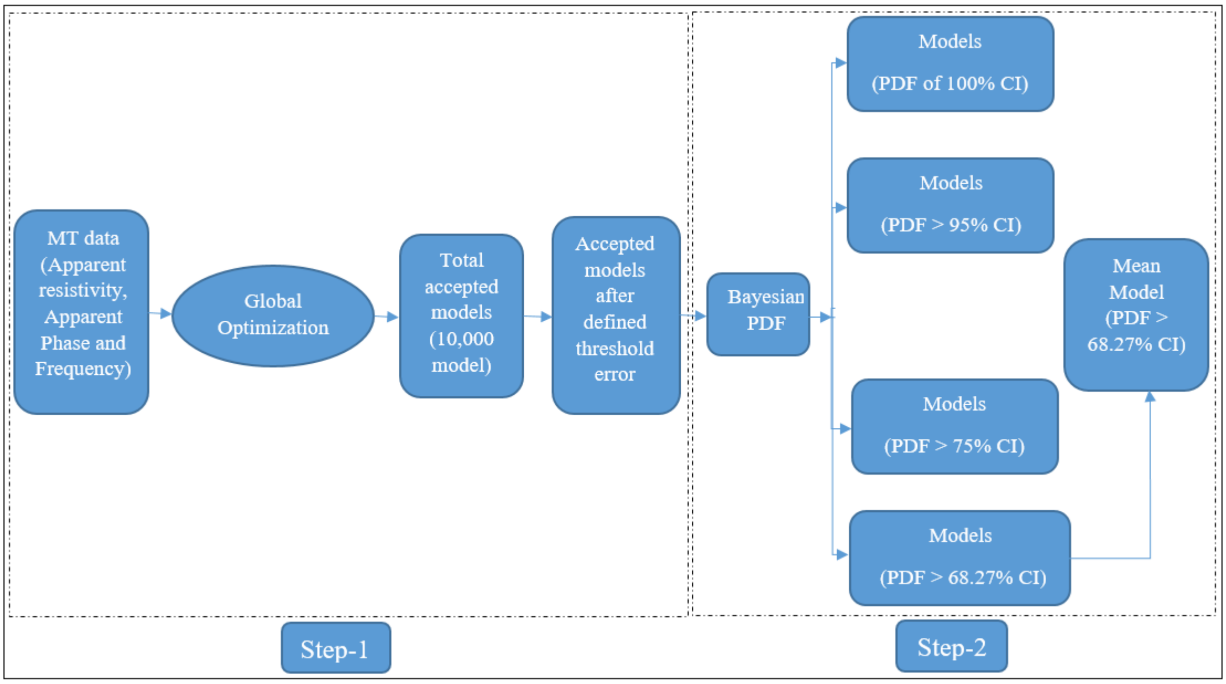

Figure 1 Schematic diagram demonstrating the essential processes considered for joint modeling of metaheuristic global optimization (Step-1) and posterior PDF technique (Step-2) for obtaining the global model by utilizing the synthetic and field MT data.

2.4 Optimization and Error Estimation

In the present study, we have implemented a new innovative global optimization technique known as wPSOGSA, in which swarm particles and mass particles provide the best particle, i.e., the best model. The best model is chosen based on the fitness of the particles, and the cost function or objective function is used to estimate this fitness. Thus magnetotelluric (MT) inverse problem can be formulated through the forward modelling operator, $f(\boldsymbol{x})$, aim at achieving the resistivity model, which illuminates the observed data ρ and φ in the foremost. This operator combines the problem of physics and inverts the observed apparent resistivity and phase data to the resistivity-depth model, $\boldsymbol{x}$**,** as:

$$(\rho, \varphi) = f(\boldsymbol{x}) \tag{7}$$

The cost function (fitness of the particle) is a mathematical relation between observed and calculated data and it is defined as the root mean square error (RMS):

$$RMS = \sqrt{\left\{\frac{(\rho-\rho_C)^2}{N} + \frac{(\varphi-\varphi_C)^2}{N}\right\}} \tag{8}$$

Where N is the total observed data points, ρ and φ are the observed apparent resistivity and phase, ρ_C and φ_C are the computed apparent resistivity and phase data.

2.5 Particle swarm optimization

The particle swarm optimization (PSO) technique is a widespread evolutionary optimization approach for determining the optimal global solution to a nonlinear inverse problem (Kennedy and Eberhart, 1995). This technique is analogous to the particle's natural behavior in search of food with the help of collaborative support from the population represented by geophysical resistivity solutions/models (known as particles) in a swarming group. The best model/position obtained among the particles so far is stored for each iteration, which helps in search for the global best solution, defined by the fitness of each particle estimated using Eq. (8). The particles' velocity and location in the search space are defined for k^{th} particle at t^{th} iteration is given below:

$$v_k(t+1) = wv_k(t) + c_1 \times rand \times \left(x_p - x_k(t)\right) + c_2 \times rand \times \left(x_g - x_k(t)\right) \tag{9}$$

$$x_k(t+1) = x_k(t) + v_k(t+1) \tag{10}$$

where w is the inertia weight set in between 0 and 1, c_1 and c_2 are a personal learning coefficient and a global learning coefficient, respectively, $v_k(t)$ is the velocity of the k^{th} particle at t^{th} iteration, and *rand* is used for a random number between 0 and 1, x_p is the present best solution. x_g is the global best solution, $x_k(t)$ is the position of the k^{th} particle at t^{th} iteration. Particles change their position at each iteration to approach an optimum solution. The first, second, and third terms in Eq. (9) represent exploratory ability, private thought, and particle collaboration, respectively.

2.6 Gravitational search algorithm

The gravitational search algorithm (GSA) is a meta-heuristic algorithm based on Newton's gravitational law (Rashedi et al., 2009), which states that mass particles attract each other with a gravitational force that is directly proportional to the product of their masses and inversely proportional to the square of the distance between them. It signifies that massive particles (here, particle represents the resistivity layer model/solution) attract to the neighboring lighter particles. Similar to PSO, the Gravitational search optimizer works with a population of particles known as mass particles in the universe. Thus the best model/solution/particle is achieved among the mass particles. The best model is defined by each particle's capability (i.e., the fitness) calculated using Eq. (8). The initialization of their position in the search spaces is given by:

$$x = rand(N, D) \times (up - down) + down \tag{11}$$

where N, D are the number of particles/models, the dimension of the model; and up, and $down$ are the upper and lower limit of the search range, respectively.

During execution time, the gravitational acting force on agent k^{th} from agent j^{th} at a specific time (t) is defined as:

$$F_{k,j}(t) = G(t)\frac{M_{p,k}(t) * M_{a,j}(t)}{R_{k,j}(t) + \epsilon}\left(x_j(t) - x_k(t)\right) \tag{12}$$

where, $M_{a,j}$, and $M_{p,k}$ are the active and passive gravitational masses for particle j and k, respectively, $x_j(t)$ is the position of the particle j at a time t for various parameters, $R_{k,j}$ (t) is Euclidian distance between two particles, and ε is a small constant.

Here, gravitational constant $G(t)$ at a specific time t is defined as (Kunche et al., 2015) and acceleration of k^{th} agent at t^{th} iteration for models is $ac_k(t)$ is defined as:

$$ac_k(t) = \frac{F_k(t)}{M_k(t)} \tag{13}$$

Where, $F_{k,j}(t)$ the gravitational acting force on agent k from agent j and $M_k(t)$ is the mass of the object at a specific time (t).

$$G(t) = G_0 \times \exp\left(-\alpha \times \frac{iter}{maxiter}\right) \tag{14}$$

where α, G_0, *iter*, and *maxiter* are descending coefficients, starting value of gravitational constant, current iteration, and maximum iterations, respectively.

The following equations are used to update the particle's velocity and location:

$$v_k(t+1) = rand \times v_k(t) + ac_k(t) \tag{15}$$

$$x_k(t+1) = x_k(t) + v_k(t+1) \tag{16}$$

All the particles are randomly placed in the search range using Eq. (11) and then initializes the particle's velocity. Meanwhile, the gravitational constant, total forces and acceleration are computed, and the locations are updated. The end criteria is the misfit error (i.e. 10^{-9}) is taken in our study.

2.7 Weighted hybrid PSOGSA (wPSOGSA)

The weighted hybrid of PSO and GSA algorithm known as the wPSOGSA algorithm integrates two essential characteristics, exploration (i.e., the ability of an algorithm to search the whole range of a given parameter) and exploitation (i.e., the ability to converge the solution nearest to the best solution) of the global optimization algorithm that increases its efficiency and converges the objective function to achieve global minima. The velocity and location of the particles updated in the wPSOGSA algorithm are illustrated in the schematic diagram (see Fig. 2).

The wPSOGSA combines the characteristic of social thinking of PSO and the searching capability of GSA; thus, the particle's velocity is defined as

$$v_k(t+1) = w \times v_k(t) + c_1 \times rand \times ac_k(t) + c_2 \times rand \times (x_g - x_k(t)) \tag{17}$$

Where $v_k(t)$ is the velocity of the particle *k* at iteration *t*, *w* is the weight function (i.e., the constant which helps to control the momentum of the algorithm to perform optimization properly), ac_k(t) is the acceleration of agent k, x_g is the best solution, and the rand is a random number lies between 0 and 1. At each iteration, particles updated their location to achieve the best solution defined as

$$x_k(t+1) = x_k(t) + v_k(t+1) \tag{18}$$

The algorithm starts by randomly initializing the velocity, mass, and acceleration of the particles. The cost function is evaluated for all particles for specified iterations to get the most optimal solution, and inverted results are updated at each iteration. Equation (12), (17), and (18) are used to update the gravitational force, velocity, and location of particles after initialization. However, the velocity and position stop updating their values when the algorithm converge and reaches the least error of the cost function.

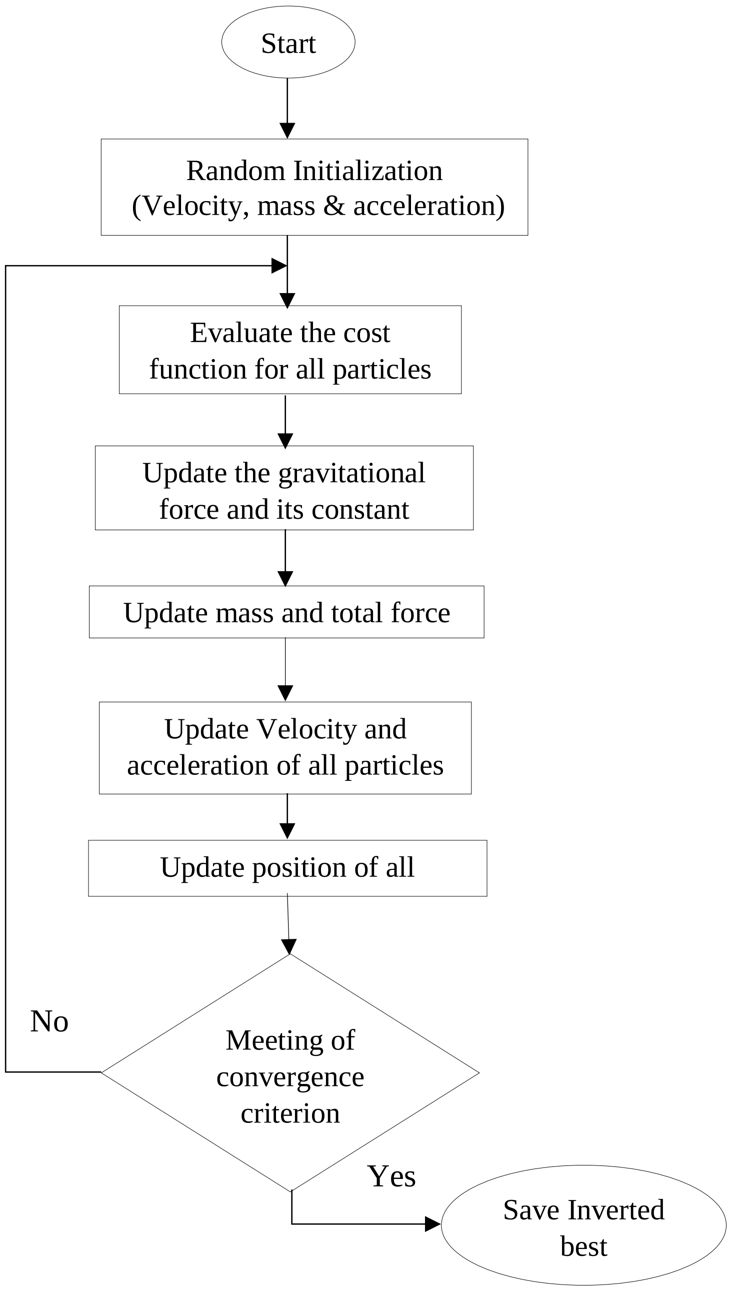

Figure 2 Flow chart of the weighted hybrid Particle Swarm Optimization and Gravity Search Algorithm known as the wPSOGSA algorithm (after (Mirjalili and Hashim, 2010)).

2.8 Bayesian probability density function

In a Bayesian framework, the probability distribution of the model parameters (known as posterior probability distribution) is computed using given observed data and models obtained from inversion. The posterior for a model is calculated using Bayes' theorem and previous model space information. Individual model parameter ranges are incorporated in the prior knowledge. The two fundamental stages in the Bayesian statistics method are the representation of previous knowledge as a probability density function and calculating the likelihood functional derived from data misfit (Tarantola and Valette, 1982). Specific characteristics, such as the best fitting model, mean model, and correlation matrix may be determined from posterior distribution of models. According to the Bayes' theorem,

$$Posterior = prior \times likelihood \tag{19}$$

As a result, our priori distribution function (f (μ)) for the parameter, x_u, mean priori information, M, and t^2 is the mean uncertainty is defined as

$$f(\mu) = \frac{1}{\sqrt{2\pi t^2}} exp\left\{-\frac{(x_u - M)^2}{2t^2}\right\} \tag{20}$$

and likelihood function is

$$f(X|\mu) = \prod_{u=1}^{n} \frac{1}{\sqrt{2\pi\sigma^2}}\ exp\left\{-\frac{(x_u - \mu)^2}{2\sigma^2}\right\} \tag{21}$$

Hence the posterior density function calculated for a parameter (x_u) using mean (μ) and variance (σ^2) defined (Lynch, 2007) as

$$f(\mu|X) = \frac{1}{\sqrt{t^2\sigma^2}}\ exp\left\{\frac{-(\mu - M)^2}{2t^2} + \frac{\sum_{u=1}^{n}(x_u - \mu)^2}{2\sigma^2}\right\} \tag{22}$$

The posterior Bayesian PDF is calculated from accepted models within a set of parameters, as shown below:

$$P(X|E) = \frac{P(X)L(E|X)}{\sum_X P(X)L(E|X)} \tag{23}$$

where, $P(X|E)$ is the posterior probability distribution of the parameter (X) given the evidence (E), $P(X)$ is the prior information of (X) and $L(E|X)$ is the likelihood function of X.

After the application of PDF, the study is further proceeded by choosing Confidence Interval (CI) of 68.27 % that is based on the empirical rule, known as the 68-95-99.7 rule (Ross, 2009). The model parameters below 68.27 % CI are discarded, and the remaining parameters are used for determining the mean model and uncertainty. Thus, the mean model (P_j) is calculated using the best models having PDF within a 68.27 % CI, defined in the following equation:

$$P_j = exp\frac{1}{Nd}\sum ln(P_{j,k}) \quad (24)$$

Here accepted models are used to calculate the correlation matrix (i.e., correlation among model parameters lie between -1 and 1) using the following equation (Tarantola, 2005):

$$CovP(l,j) = \frac{1}{Nd}\sum(P_{l,k} - P_l)(P_{j,k} - P_l) \quad (25)$$

and

$$CorP(l,j) = \frac{CovP(l,j)}{\sqrt{CovP(l,l) \times CovP(j,j)}} \quad (26)$$

Here, N is the total number of models, d is used for the number of the layer parameters, $P_{j,k}$ is the j^{th} model parameter of k^{th} model where l and j both vary from 1 to d (number of layer parameters). $CovP(l,j)$ is the covariance matrix between model parameter l and j, $P_{l,k}$ is the model parameter l^{th} model parameter of k^{th} model and $CorP(l,j)$ is the correlation matrix between model parameter l and j.

3.0 Results and analysis

The effectiveness, sensitivity, stability, and robustness of the proposed wPSOGSA algorithm in identifying the authentic subsurface structure are evaluated using various MT datasets. These datasets consist of synthetic data with no noise and Gaussian noise, which simulate different geological formations. Additionally, two MT field datasets have been optimized for analysis.

3.1 Application to synthetic MT data-Three layers case

This synthetic MT data that was executed for 10000 runs keeping the same lower and upper bounds as given in Table 1, and iteration to 1000. Figure 3 shows (a) the observed apparent resistivity with the computed data, (b) the observed apparent phase with the computed data, (c) 1D inverted model by wPSOGSA (red color), GSA (green color) and PSO (blue color) with a true model (black color), and 2(d) shows the relation between misfit and iterations for the noise-free synthetic data.

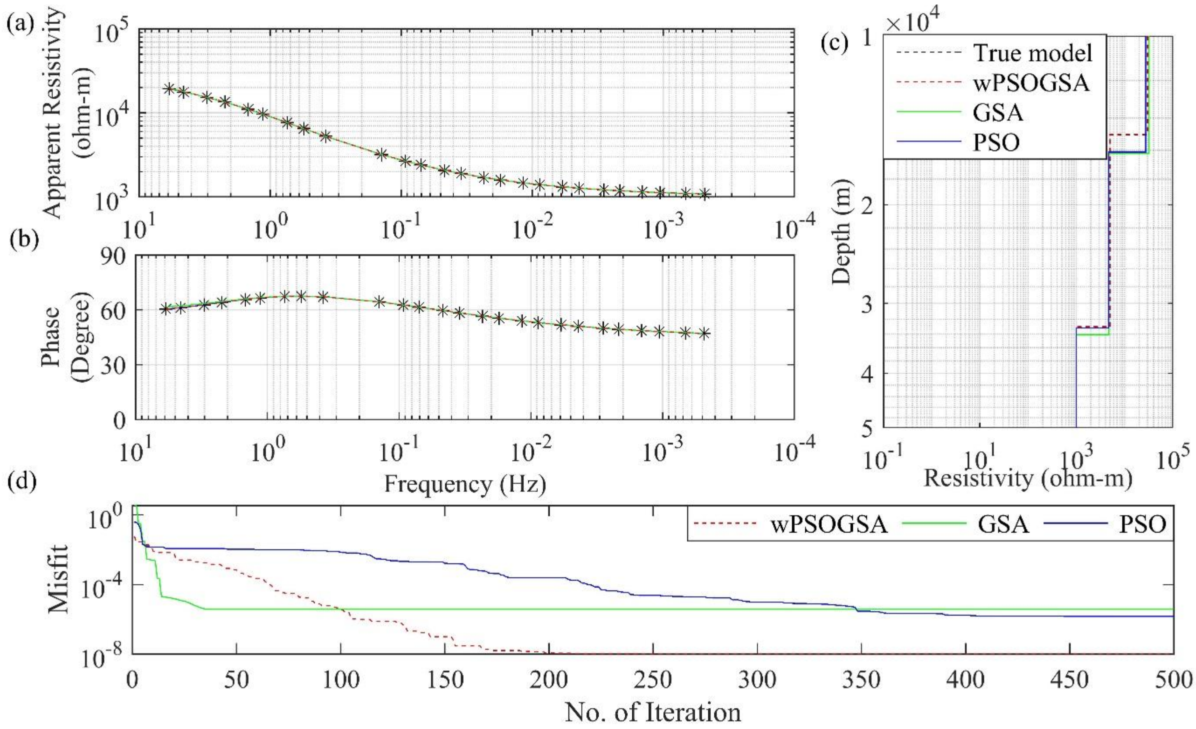

Figure 3 The inverted MT response by PSO (blue color), GSA (green color), and hybrid wPSOGSA (red color) with a true model (black color) over three-layer synthetic data as shown in (a) observed and calculated apparent resistivity curve, (b) observed and calculated apparent phase curve, (c) 1D depth inverted model, and (d) misfit error versus iterations.

The misfit curve as shown in Fig. 3(d) is gradually decreasing with increasing iterations and becomes constant, where the algorithm converges. The PSO, GSA, and wPSOGSA converge at iterations 492, 35, and 316 with associated errors 1.51e-6, 3.97e-6, and 1.035e-8, and the associated computational time is 27.06 seconds, 1.75 seconds, and 3.35 seconds, respectively. Thus, the curves describes that wPSOGSA converges at the least RMS error. Whereas PSO, GSA, and wPSOGSA using 10 % noisy synthetic data converge at 102, 88, and 358 iterations with an associated error are 0.00435, 0.00439, and 0.00426, and associated computational times are 5.61 seconds, 4.40 seconds, and 3.80 seconds, respectively.

The 20 % noisy synthetic MT data that was executed for 10000 runs keeping the same lower bound, upper bound, and iteration. The well fitted inverted MT response (see Fig. 4) as follows: (a) the corrupted synthetic and calculated apparent resistivity data, (b) the corrupted synthetic and calculated apparent phase data, (c) the inverted 1D depth model, and (d) convergence response in terms of misfit error versus iterations. We analyzed Fig. 4(d) and found that the PSO, GSA, and wPSOGSA using noisy synthetic data converge at iterations 236, 7, and 73 with associated errors 0.0394, 0.0408, and 0.0393, respectively.

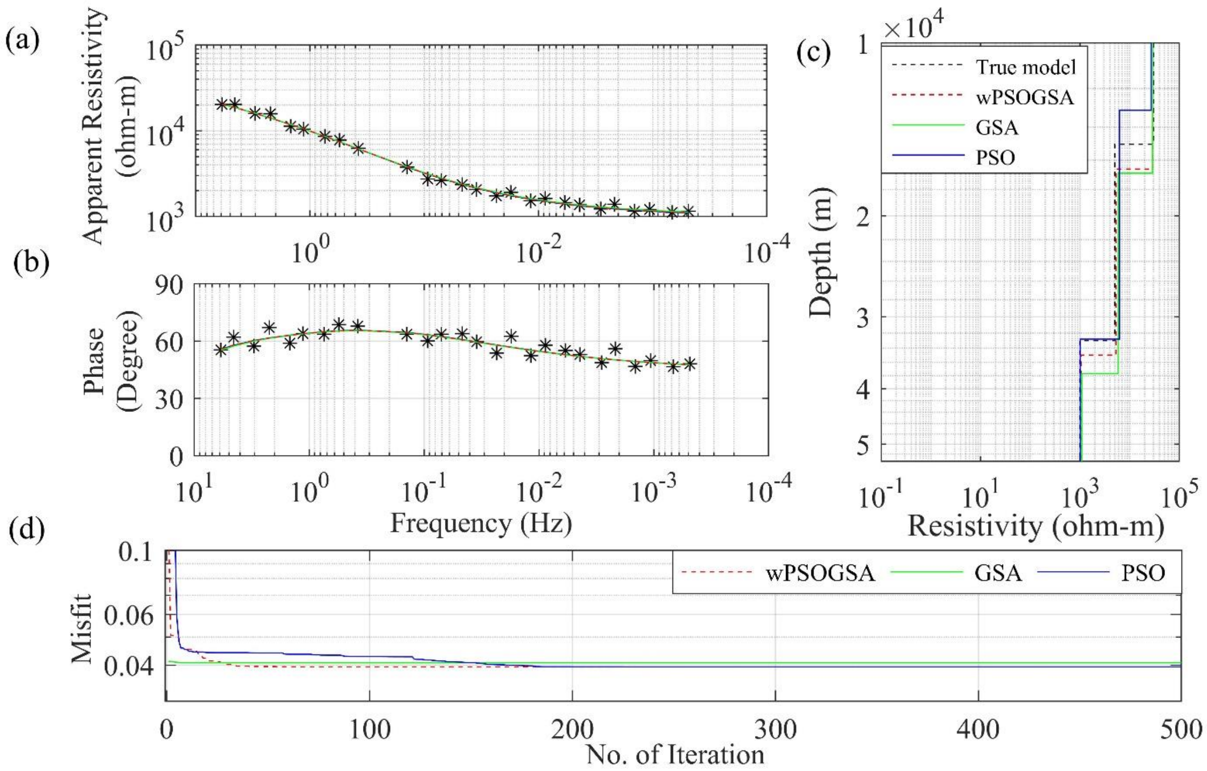

Figure 4 The inverted MT response by PSO (blue color), GSA (green color), and hybrid wPSOGSA (red color) with a true model (black color) over three-layer synthetic data with 20 % random noise as shown in (a) observed and calculated apparent resistivity curve, (b) observed and calculated apparent phase curve, (c) 1D depth inverted model, and (d) misfit error versus iterations.

3.1.1 Bayesian analysis and uncertainty in model parameters

Two methods are used to estimate mean solution and uncertainty: one method is the mean solution for all accepted best-fitted solutions acquired from 10,000 runs for all three global optimization techniques; another method is the model derived from all approved solutions using posterior Bayesian PDF within one standard deviation. To get the global best solutions in our study, we incorporated posterior PDF based on the Bayesian approach to enhance the efficacy of the inverted model and minimize the uncertainty in the model. The process for obtaining the mean solution is proceeded by selecting an initial threshold error which is essential because smaller the threshold value, more significant number of models with lesser uncertainty in the model parameters (Sharma, 2012). Thus, a more considerable threshold gives a lesser number of models with enormous uncertainty in the model parameter (Sen and Stoffa, 1996; Sharma, 2012). This is further proceeded by calculating the PDF for each parameter value using Eq. (22). In order to select values of each parameter that having higher posterior PDF, a 68.27 % CI is used. The mean model obtained from selected model parameters is near to the actual model.

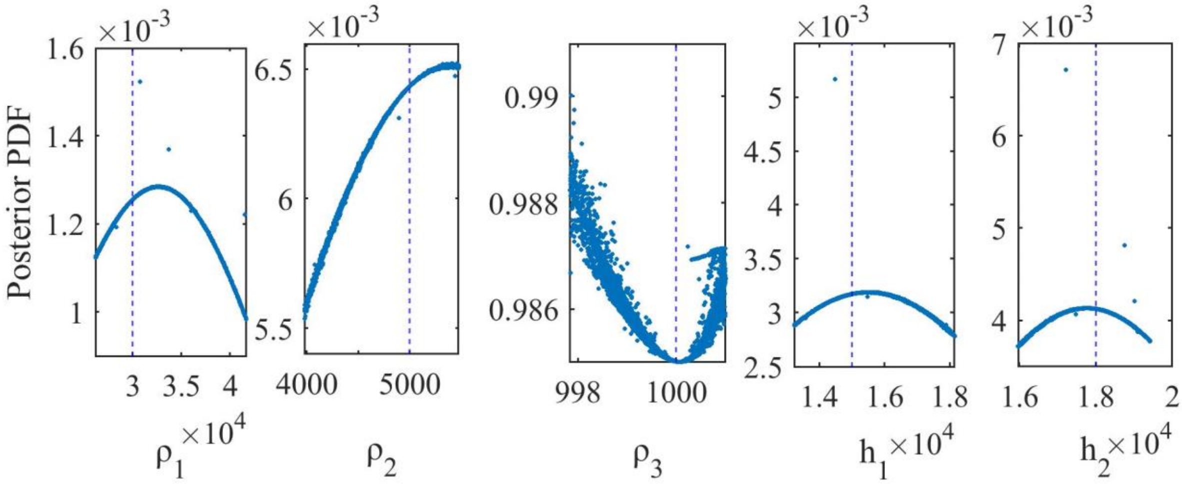

Figure 5 Posterior Bayesian probability density function (PDF) with 68.27 % CI for wPSOGSA for three-layered synthetic data.

Figure 5 shows the output of posterior Bayesian PDF, which select model parameters with lesser error. The straight lines (dashed lines) present the actual value of the respective layer parameters. The first layer thickness, second layer thickness, and first layer resistivity have higher uncertainties, i.e., 61.25 m, 51.47 m, and 210.61 Ωm, respectively, whereas the second layer resistivity and third layer resistivity have lower uncertainty, i.e., 17.71 Ωm and 0.03 Ωm, respectively.

Table 1 True model, search range, and inverted layer parameters by hybrid wPSOGSA, GSA, and PSO for three-layer with different noise (0 %, 10 %, and 20 %) synthetic MT apparent resistivity and apparent phase data.

Layer parameters		ρ_1 (Ωm)	ρ_2 (Ωm)	ρ_3 (Ωm)	h_1 (m)	h_2 (m)
True model		30000	5000	1000	15000	18000
Search Range		5000 - 50000	1000 - 10000	50 - 5000	5000 - 25000	10000-25000
(Shaw & Srivastava, 2007) 2.0 % Gaussian random noise	PSO	26981.80	6230.30	1011.70	13090	19720
	GA	40800	10000	1010	6210	25000
	RR	43424.40	3097.10	980.70	17010.00	16960.00
0 % noisy data	PSO	27463.86	4664.57	999.48	16112.66	17080.01
	GSA	32017.78	4721.69	1004.05	16195.26	17928.07
	wPSOGSA	30243.42	5007.04	1000.02	14969.33	18029.76
10 % noisy data	PSO	19861.54	7659.73	1022.19	15971.66	14774.31
	GSA	27538.91	6534.61	1018.04	14117.82	17408.14
	wPSOGSA	27589.85	6043.87	998.99	14902.89	18221.87
20 % noisy data	PSO	26981.8	6230.3	1011.7	13090.00	19720.00
	GSA	28823.57	5825.19	1089.65	16861.84	20795.48
	wPSOGSA	29208.75	5282.77	1055.09	16573.22	18398.94

Table 1 shows the inverted layer parameters using wPSOGSA, GSA, and PSO for noise-free and noisy synthetic MT data based on posterior Bayesian PDF, as well as the actual model and the search range. In addition, layered properties of synthetic data corrupted with 10 % and 20 % random noise are compared and statistically analyzed. Our findings, as shown in Table 1, were compared to those obtained using the Genetic Algorithm (GA), Ridge Regression (RR), and PSO by (Shaw and Srivastava, 2007)), which consistently outperforms GA and RR is closer to the genuine model.

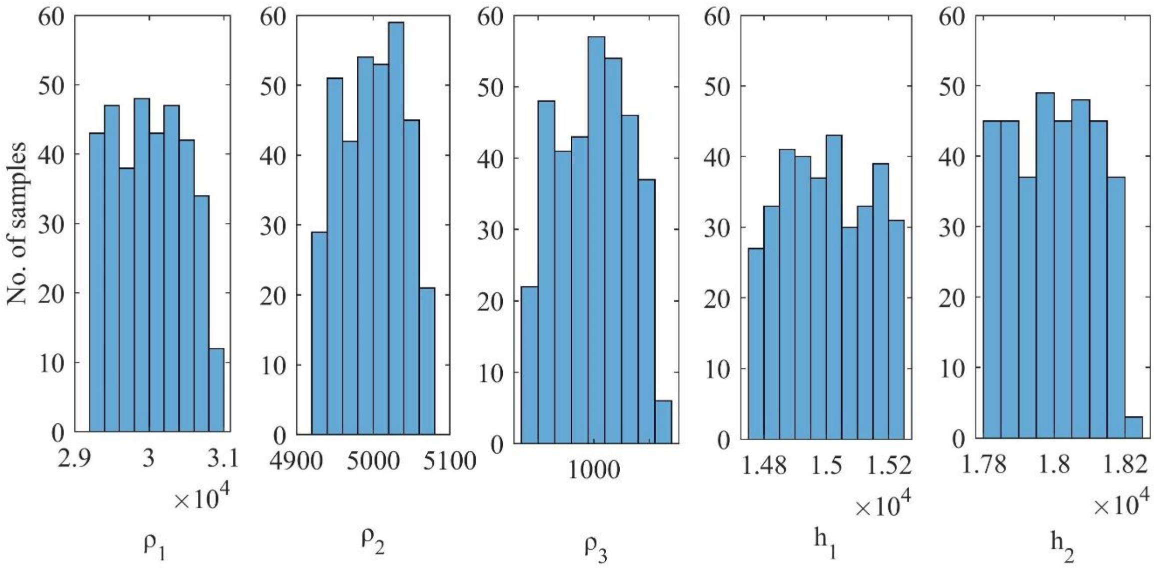

Figure 6 Histogram of selected models for misfit error below a defined threshold error of wPSOGSA.

Mean value of the accepted model parameters (30243.42±471.26, 5007.04±39.59, 1000.02±0.064, 14969.33±136.82, 18029.76±114.90) with high uncertainty of the parameters (1.5 %, 0.78 %, 0.0064 %, 0.91 % and 0.63 %). On the basis of low posterior PDF and high uncertainty, we have taken (ρ_1) and (h_1) for the exercise to show the models are not biased to the selected models.

As well as based on the histograms (see Fig. 6), posterior PDF and uncertainty of the inverted layer parameters resistivity (ρ_1) and thickness (h_1) for the three-layered synthetic MT data have been taken to depict the global solution using presented algorithm. Here we prepared the cross-plots of ρ_1 versus h_1 using (a) wPSOGSA, (b) PSO, and (c) GSA, showing all accepted models (red circle), selected models with misfit error less than a threshold error of 10^{-4} (magenta circle), models of a PDF greater than 95 % (blue circle), models of a PDF greater than 75 % (green circle), models of a PDF greater than 68.27 % (yellow circle), and mean model, i.e., model parameters which having a PDF greater than 68.27 % (black asterisk) as shown in Fig. 7. It is noticed that all inverted results give the global solution which has a good agreement with the true model, whereas wPSOGSA gives the more accurate results than the other two algorithms PSO and GSA as shown in Table 2.

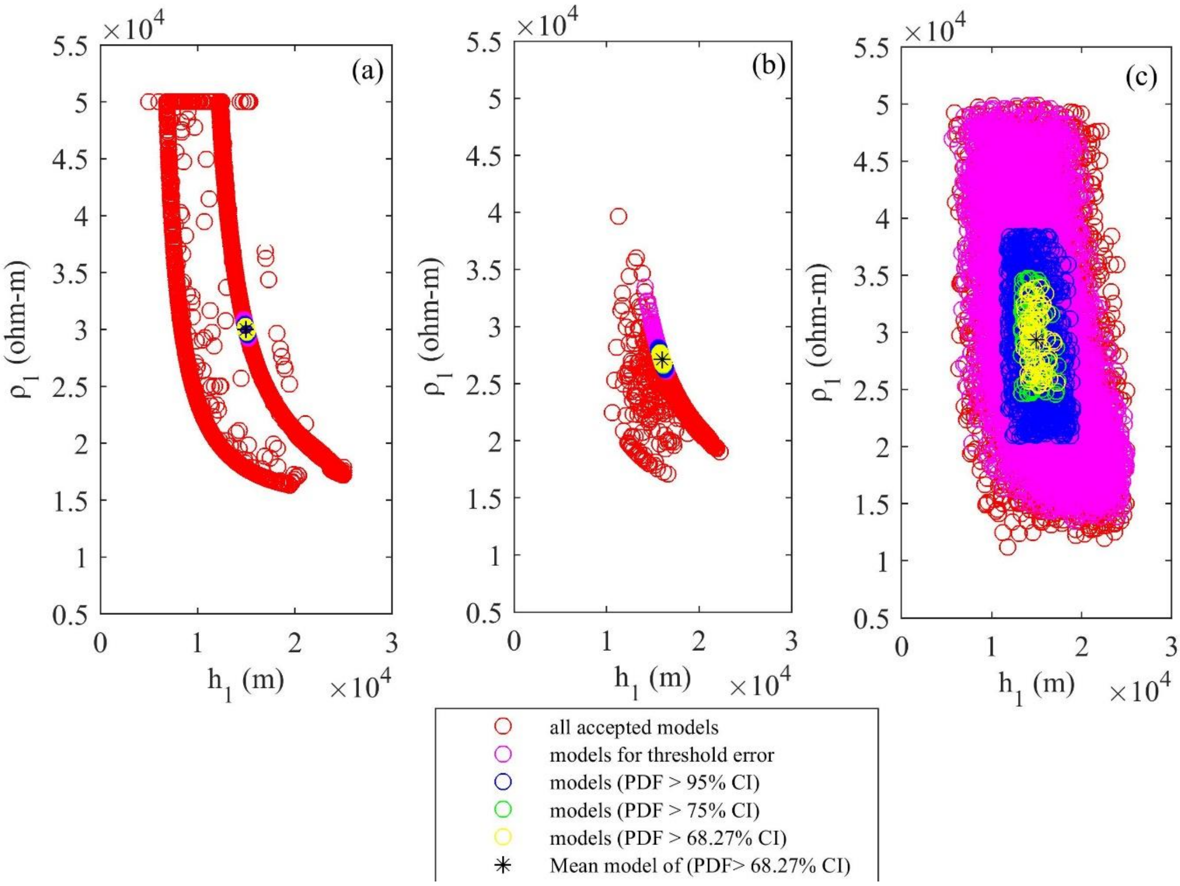

Figure 7 Cross-plots of thickness and resistivity of first layer for the three-layered synthetic resistivity model using (a) wPSOGSA, (b) PSO, and (c) GSA, displaying all accepted models (red circle), selected models with misfit error less than a threshold error (magenta circle), models (pdf > 95 % CI, blue circle), models (pdf > 75 % CI, green circle), models (pdf > 68.27 % CI, yellow

circle), and mean model i.e. model parameters which having a PDF greater than 68.27 % (black asterisk).

3.1.2 Sensitivity, correlation matrix, and model parameters

The accepted models, which have posterior PDF value within 68.27 % CI, are used to calculate the correlation matrix. This correlation matrix gives the relationship among model parameters. Thus, the lesser correlation value gives weak relation among the parameters and vice versa. The correlation matrix of PSO, GSA, and wPSOGSA was examined on one set of synthetic data, as shown in Fig. 8, Fig. 9 and Fig. 10, demonstrating the sensitivity among inverted model parameters. The value of correlation matrix, 1.0 indicates that the two parameters are strongly correlated.

Figure 8 shows that first layer resistivity is correlated highly positively with a first-layer thickness (0.97) and second layer thickness (0.98), while the second layer resistivity (-0.99) and third layer resistivity (-0.81) are substantially negative connected. Second layer resistivity is correlated with the third layer resistivity (0.87) which has a significant positive relationship; while second layer resistivity has a significant negative correlation with the first layer thickness (-0.99) and the second layer thickness (-1.00). First layer thickness (-0.92) and second layer thickness (-0.90) are very negatively associated with third layer resistivity, while first layer thickness is extremely positively correlated with a second layer thickness (0.99).

Figure 9 indicates that first layer resistivity is highly associated with a second layer thickness (1.00) and weakly with second layer resistivity (-1.00), third layer resistivity (-1.00), and first layer thickness (-1.00). Second layer resistivity (-1) is highly linked with a second layer thickness (-1.00), while third layer resistivity (1.00) and first layer thickness are strongly correlated (1.00). Third layer resistivity has a highly positive correlation with a first-layer thickness (1.00) and a strong negative correlation with a second layer thickness (-1.00), whereas first layer thickness has a significant negative correlation with a second layer thickness (-1.00).

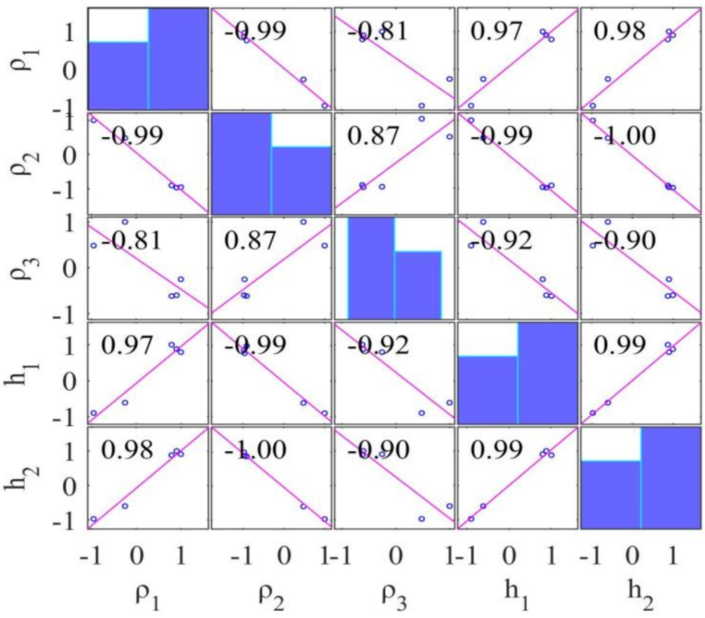

Figure 8 Correlation matrix calculated from PSO inverted model using a three-layer noise-free synthetic MT apparent resistivity and apparent phase data.

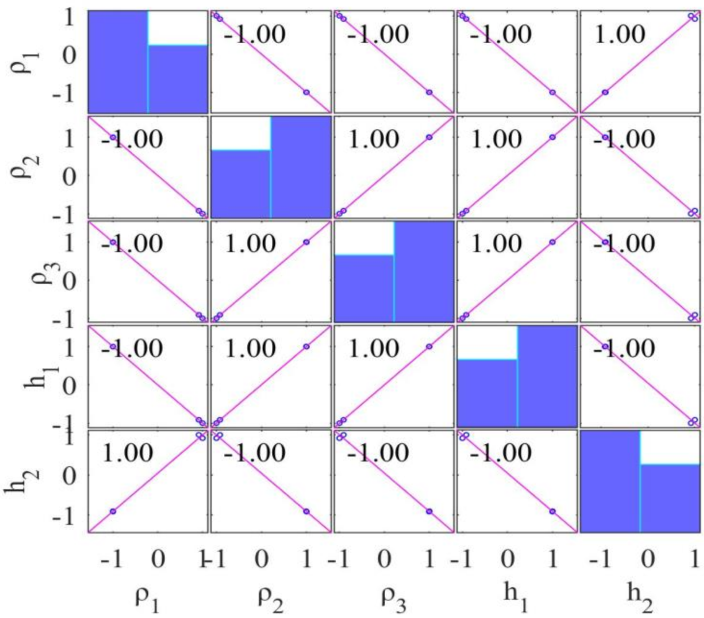

Figure 9 Correlation matrix calculated from GSA inverted model using a three-layer noise-free synthetic MT apparent resistivity and apparent phase data.

Figure 10 shows the correlation matrix of wPSOGSA. The analyses reveal that the first layer resistivity is strongly negative with the second layer resistivity, substantially negative (-0.92) with the third layer resistivity, weakly positive (0.30) with the first layer thickness, and considerably (0.63) with the second layer thickness. Second layer resistivity is slightly positive (0.31) when compared to third layer resistivity (0.43) but substantially negative when compared to first layer thickness. Third layer resistivity has a slightly negative correlation (-0.23) with first layer thickness, but a moderately negative correlation (-0.71) with second layer thickness and first layer thickness has a negative correlation (-0.71). Thus, the conclusion can be made that the layer parameters are independent of others, so changing one will have no effect on the other compared to the result obtained via PSO and GSA algorithms.

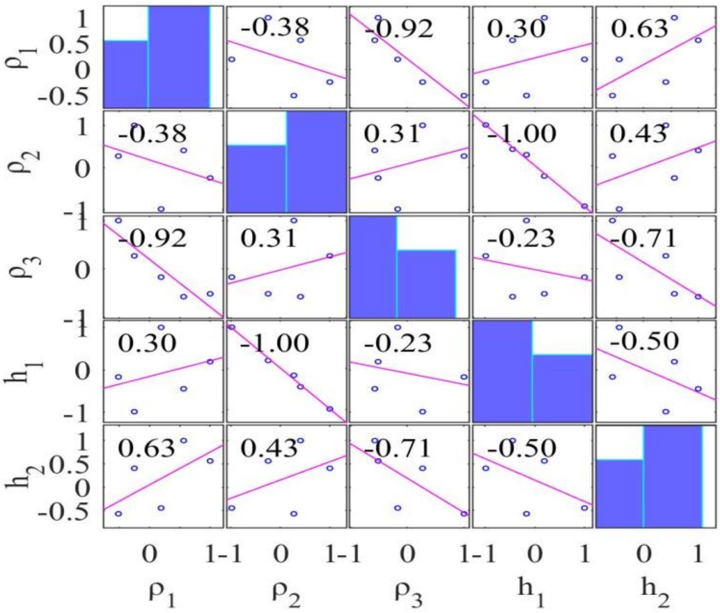

Figure 10 Correlation matrix calculated from wPSOGSA inverted model using a three-layer noise-free synthetic MT apparent resistivity and apparent phase data.

3.1.3 Stability analysis

We used two different search ranges for stability evaluation of proposed wPSOGSA algorithms and executed the algorithms over three layers of synthetic MT data. One of which is expanded, and the other is contracted by 10 % of the initial search range. We infer from three layers of synthetic data, results fluctuate by approximately 3 % from the true value when the search range is changed. This variation is about 10 % on average for synthetic data corrupted with 30 % random noise, as shown in Table 2.

Table 2 Stability analysis of a hybrid algorithm for three layers of synthetic data.

Layer parameters		ρ_1 (Ωm)	ρ_2 (Ωm)	ρ_3 (Ωm)	h_1 (m)	h_2 (m)
Search Range		5000-50000	1000-10000	50-5000	5000-25000	10000-25000
Search Range - Case 1		4500-55000	900-11000	45-5500	4500-27500	9000-27500
wPSOGSA inverted model	0 %	31092.47	5085.79	1000.14	14700.83	18251.85
	30 %	30113.82	5016.75	1137.05	15880.95	23970.22
Search Range - Case 2		5500-45000	1100-9000	55-4500	5500-22500	11000-22500
wPSOGSA inverted model	0 %	29078.26	4922.85	999.91	15273.25	17767.45
	30 %	27815.97	5464.88	1156.46	17398.41	18119.61

3.2 Application to synthetic MT data-Four layers case

For the second example of the synthetic data, a typical four-layer HK-type of earth model to analyse the performance of the present algorithm with Improved Differential Evolution (IDE) results obtained by Xiong et al. (2018). Analysis over noisy synthetic data is done by corrupting synthetic data with 10 % and 20 % Gaussian random noise to mimic the real field data because different types of noises influence apparent resistivity data. Following that, all three optimization methods are run using the noisy synthetic data. As the misfit error increases with the noise in the data, the Bayesian PDF of 68.27 % CI is calculated with respect to the threshold misfit error of 0.01 and thus the mean model is calculated.

Enormous uncertainty is shown in the inverted results; hence, we calculated the mean model for 68.27 % CI using posterior Bayesian PDF to reduce the uncertainty and produce the global best solution. The optimized results obtained from the posterior PDF and the true model are shown in Table 3. Figure 11 illustrate the inverted responses for PSO, GSA, and wPSOGSA are well-fitting as follows (a) observed and calculated apparent resistivity data, (b) observed and calculated apparent phase data, (c) 1-D depth model, and (d) convergence response of present algorithms. We have estimated the layer parameters for synthetic data corrupted with 20 % random noise for comparative analysis and found that the PSO, GSA, and wPSOGSA converge at iterations 96, 556, and 187 with associated errors 3.69, 4.04, and 3.69, respectively.

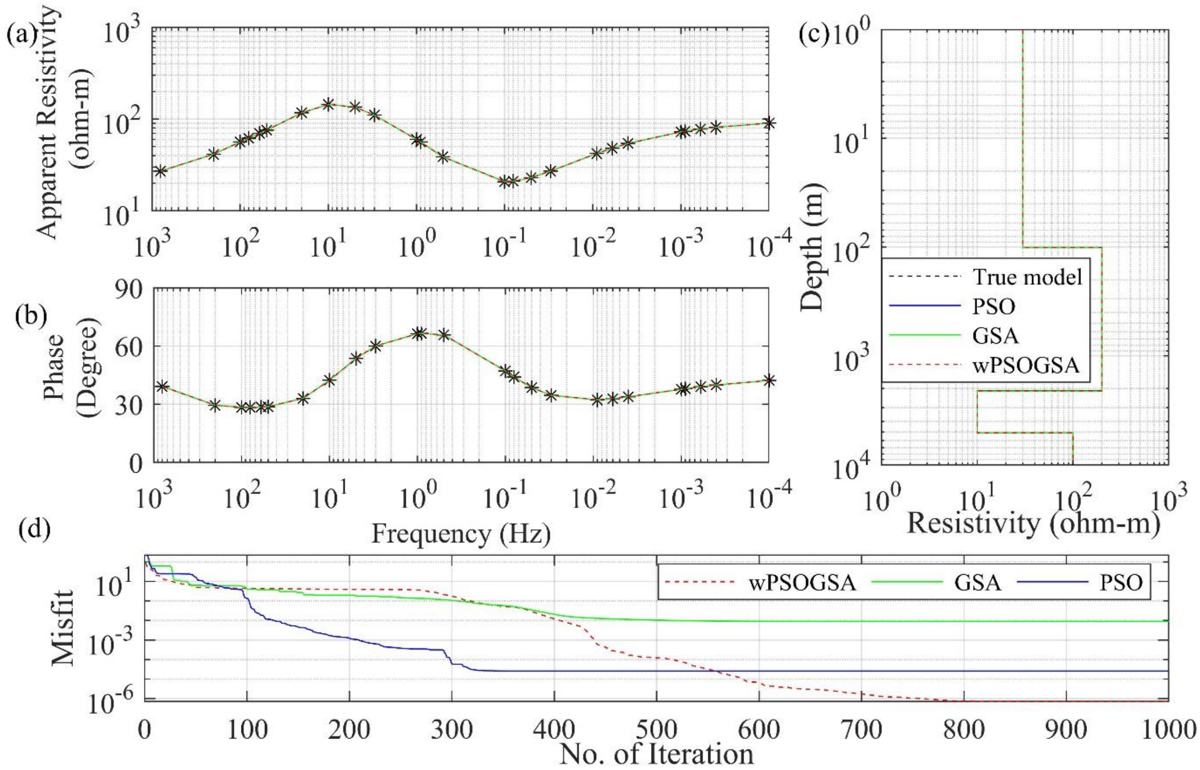

Figure 11 The inverted MT response by PSO (blue color), GSA (green color), and hybrid wPSOGSA (red color) with a true model (black color) over four-layer synthetic data as shown in (a) observed and calculated apparent resistivity curve, (b) observed and calculated apparent phase curve, (c) 1D depth inverted model and (d) convergence curve.

Additionally, the synthetic data corrupted with 10 % random noise is also used for the execution of inversion keeping the search range, a number of particles, and iterations same as before, and observed that the PSO, GSA, and wPSOGSA converge at iterations 151, 2 and 250 with associated error 1.7609, 1.95 and 1.76 respectively. The posterior Bayesian PDF for threshold data with 68.27 % CI is calculated similarly as a three-layer case to minimize the uncertainty in inverted results.

Table 3 Comparison of the result obtained from improved Differential Evolution (IDE) and inverted results of PSO, GSA, and hybrid wPSOGSA obtained by using posterior PDF for four-layer synthetic apparent resistivity data with different Gauss noise levels (0 %, 10 %, and 20 %) and True model.

Layer parameters		ρ_1 (Ωm)	ρ_2 (Ωm)	ρ_3 (Ωm)	ρ_4 (Ωm)	h_1 (m)	h_2 (m)	h_3 (m)
True model		30.00	200.00	10.00	100.00	100.00	2000.00	3000.00
Search Range		25-35	100-250	5-15	50-150	50-200	1000-3000	2000-3500
0 % noise	IDE	30.00	200.00	9.99	100.01	100.00	1991.98	3000.24
	PSO	30.00	200.001	10.00	100.00	100.00	2000.00	3000.00
	GSA	29.95	199.79	9.99	99.99	99.67	2000.70	2995.37
	wPSOGSA	30.00	200.00	10.00	100.00	100.00	2000.00	3000.00
10 % noise	IDE	30.24	210.28	08.92	99.67	109.83	1994.63	2667.13
	PSO	32.86	224.99	11.51	107.65	109.71	1971.78	3499.92
	GSA	29.77	209.78	9.50	106.78	92.38	2073.14	2754.77
	wPSOGSA	30.46	197.18	9.97	102.01	100.50	1974.83	3079.35
20 % noise	IDE	30.30	212.41	11.44	97.92	102.40	1930.17	3347.24
	PSO	34.99	247.04	11.80	114.56	115.16	1986.08	3499.99
	GSA	29.52	225.61	9.74	113.46	87.55	2081.26	2753.29
	wPSOGSA	34.88	246.08	11.75	114.54	114.58	1990.98	3489.10

3.2.1 Stability analysis

For the stability evaluation of presented algorithms over four layers of synthetic MT data, similar to the three-layer case, we used two different search ranges and executed the algorithms for 1000 iterations. The method exhibits good results with four layers of synthetic data and reveals minimal variation for noise-free data. For 30 % contaminated data, the variation is approximately 10 % and 12 % in case 1 and case 2, respectively. The outputs don't change much across runs and provide consistent results, as shown in Table 4.

Table 4 Stability analysis of a hybrid algorithm for four layers of MT synthetic data.

Layer parameters		ρ_1 (Ωm)	ρ_2 (Ωm)	ρ_3 (Ωm)	ρ_4 (Ωm)	h_1 (m)	h_2 (m)	h_3 (m)
Search Range		25-35	100-250	5-15	50-150	50-200	1000-3000	2000-35000
Search Range-Case 1		27.50-31.50	110-225	5.50-13.50	55-135	55-180	1100-2700	2200-3150
wPSOGSA inverted model	0 %	29.99	199.99	10.00	99.99	99.99	1999.99	3000.00
	30 %	31.5	220.79	11.17	109.18	99.48	2150.07	3150
Search Range-Case 2		22.50-38.50	90-275	4.50-16.50	45-165	45-220	900-3300	1800-3850
wPSOGSA inverted model	0 %	29.99	199.99	10.00	99.99	99.99	1999.99	3000.00
	30 %	35.47	264.27	11.95	103.13	116.22	2020.37	3040.95

3.3 Application to field MT data-Island of Milos, Greece

In one-dimensional MT data for site G5 near borehole M2 (Hutton et al., 1989), as shown in Fig. 12, the apparent resistivity and phase values are inverted using the wPSOGSA, PSO, and GSA, keeping the same set of controlling parameters as for noisy synthetic data, such as the swarm size, inertia weight (w), personal learning coefficient (c_1) and a global learning coefficient (c_2), descending coefficient (α), and the initial value of universal gravitational constant (G_0).

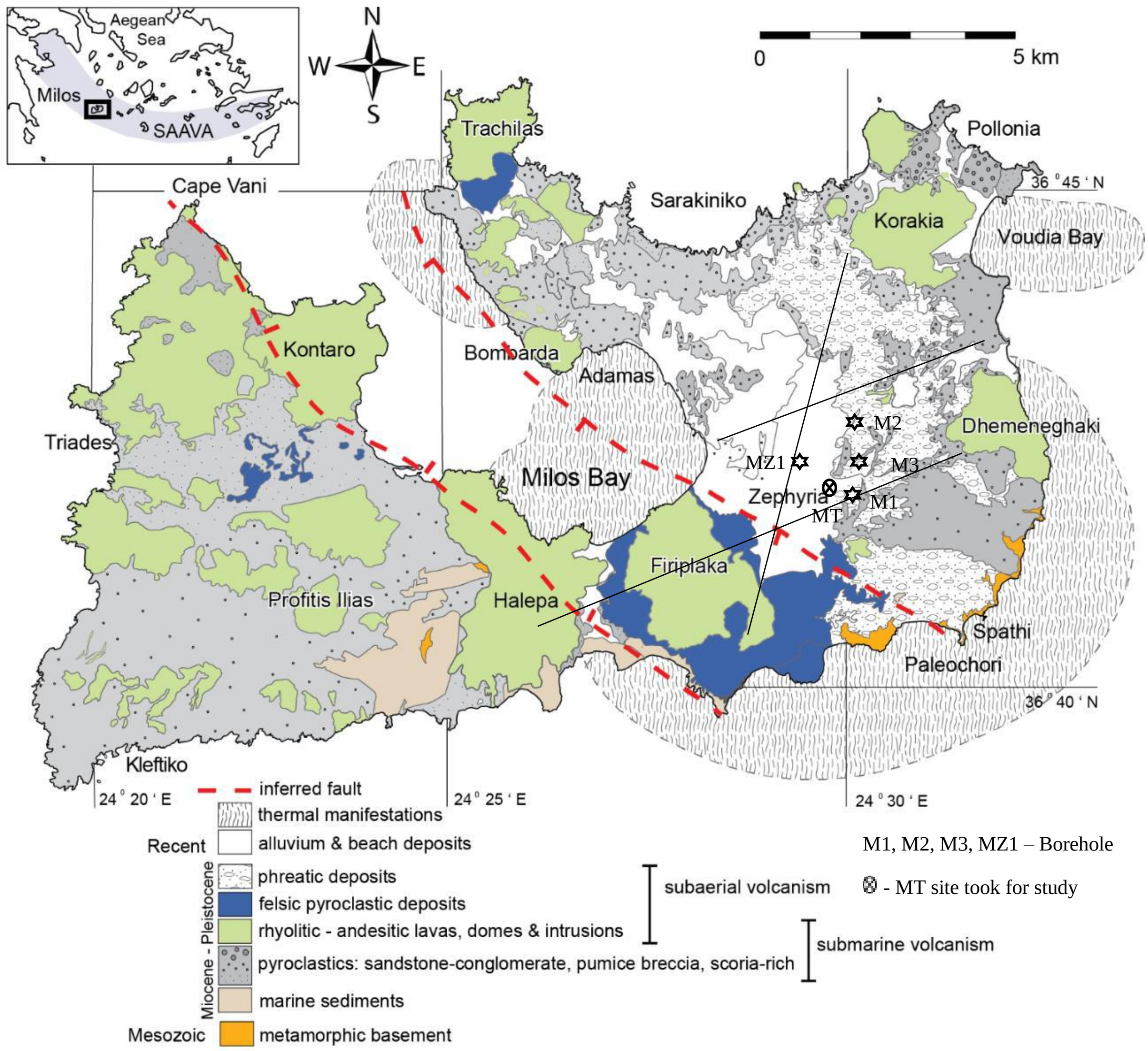

Figure 12 The location of the MT site and geology of the Island of Milos, Greece (after (Stewart and McPhie, 2006)).

Figure 13 shows the calculated data and model parameters as (a) match between observed and computed apparent resistivity data, (b) match between observed and computed apparent phase data, and (c) 1D inverted model and (d) convergence response of wPSOGSA (red color), GSA (green color), and PSO (blue color) along with true model (black color). In subfigure Fig. 13(c) depicts alluvium deposits with a resistivity of 1.0 Ωm with 15 m thickness as the top layer, and volcanic deposits with a resistivity of 300 Ωm and 10 m thickness lie beneath the alluvium deposits. A very high conducting layer of resistivity less than 1.0 Ωm is estimated, equivalent to the green lahar under the high resistivity volcanic deposits. The next layer below, with higher resistivity, corresponds to the crystalline foundation. In the geothermal zone's depths, the resistivity drops again. The resistivity in the depth range of about 1000 m, which is similar to earlier studies, was explored, and the findings of the proposed algorithm discovered to be in good agreement with model developed by Dawes in Hutton et al. (1989).

In subfigure Fig. 13(d) reveals that the algorithms converge at iterations 218, 1, and 425 with corresponding errors of 0.0494, 0.0518, and 0.0493 for PSO, GSA, and wPSOGSA, respectively. The hybrid algorithm has the least error between observed and computed data. The algorithms are executed for 1000 iterations and 10000 models, and findings are compared with available stratigraphy, and the result is derived using the Monte-Carlo technique by Hutton et al. (1989). After examining our optimized effects from Fig. 13 and Table 5, hybrid wPSOGSA outperformed PSO and GSA.

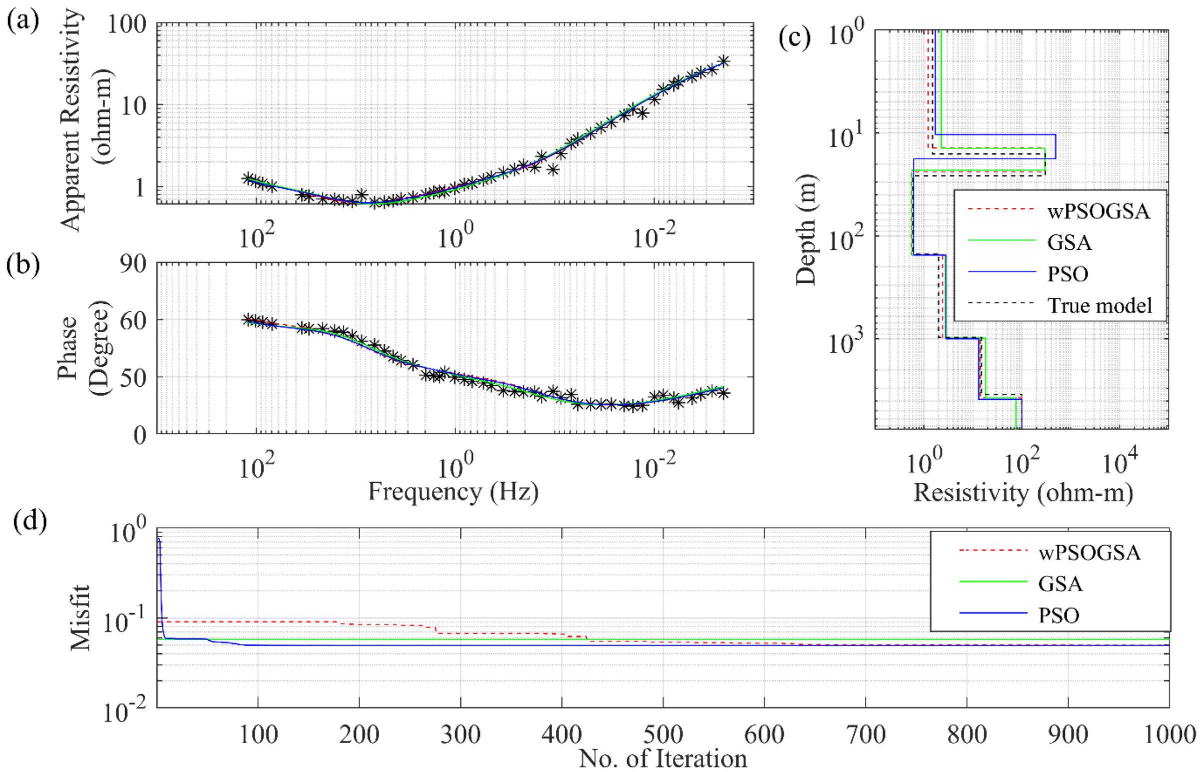

Figure 13 The inverted MT response by PSO (blue color), GSA (green color), and hybrid wPSOGSA (red color) with a true model (black color) over the geothermal area, Island of Milos, Greece, as shown in (a) observed and calculated apparent resistivity curve, (b) observed and calculated apparent phase curve, (c) 1D depth inverted model and (d) convergence curve.

3.3.1 Bayesian analysis and uncertainty in model parameters

A posterior Bayesian method determines the global model and related uncertainty. Figure 14 shows another uncertainty study that examined the six-layered resistivity model over the geothermal field, Island of Milos, Greece, and found that the peak values of the posterior PDF for all model parameters are very nearer to the actual value of the layer parameters, providing less uncertainty. We have analyzed the wPSOGSA inverted results from the Fig. 14 and Table 5, and found that the first, second, third, fourth, fifth, and sixth layers' resistivity with uncertainty in associated layer parameters is 1.23±0.49 Ωm, 297.61±53.43 Ωm, 0.55±0.02 Ωm, 2.41±0.16 Ωm, 14.18± 1.76 Ωm and 99.92±0.37 Ωm. Similarly, the associated thicknesses with uncertainty are 14.51±1.35 m, 9.85±1.35 m, 127.39±6.01 m, 823.01±7.57 m and 2750.88±63.07 m. Thus, the analysis suggests the lesser uncertainties in each layer's parameters except resistivity of the first and second layers.

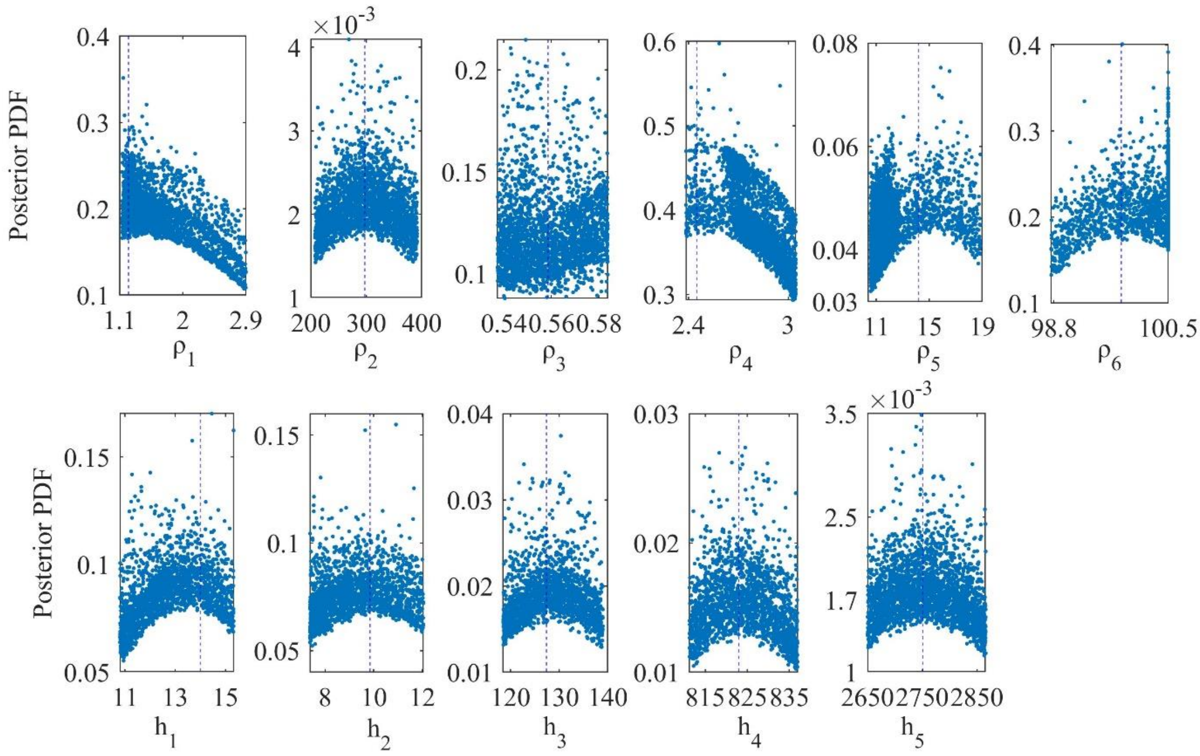

Figure 14 Posterior Bayesian probability density function (PDF) with 68.27 % CI for wPSOGSA over a geothermal field, Island of Milos, Greece.

Table 5 compares optimized results obtained from all three presented algorithms based on posterior Bayesian PDF under 68.27 % CI condition. However, the 1D depth model inverted from wPSOGSA shows good agreement with the available borehole M-2 (Hutton et al., 1989). As a result, the hybrid algorithm is functioning better and the findings are encouraging.

Table 5 Search range and inverted results by posterior PDF (68.27 % CI) and PSO, GSA, and hybrid wPSOGSA for six-layered field data.

Layer parameters		ρ_1 (Ωm)	ρ_2 (Ωm)	ρ_3 (Ωm)	ρ_4 (Ωm)	ρ_5 (Ωm)	ρ_6 (Ωm)	h_1 (m)	h_2 (m)	h_3 (m)	h_4 (m)	h_5 (m)
Search Range		0.1-5	50-500	0.1-5	1-10	10-30	50-100	10-20	5-15	110-150	800-850	2500-3000
Mean Posterior	PSO	1.71	493.81	0.62	2.82	13.22	99.97	10.39	7.44	135.4	843.77	2861.35
	GSA	2.28	299.28	0.54	2.76	18.25	76.03	14.08	8.81	130.75	825.32	2753.07
	wPSOGSA	1.23	297.61	0.55	2.41	14.18	99.92	14.51	9.85	127.39	823.01	2750.88

3.3.2 Sensitivity, correlation matrix, and model parameters

Here, a similar study of the correlation matrix is carried out for field example from the Island of Milos, Greece using all accepted models, which have posterior PDF values within 68.27 % CI. The correlation matrix of PSO, GSA, and wPSOGSA was examined over the field MT data as shown in Fig. 15, Fig. 16 and Fig. 17 demonstrating the sensitivity among inverted model parameters and found an almost similar correlation among the layer parameters for three-layer synthetic study. From correlation analyses, we noticed that the values are showing moderate and weak correlation among parameters in the wPSOGSA case, indicating that wPSOGSA is linearly independent of layer parameters. This indicates that the parameter is less affected by other layer parameters and resistivity curves. Whereas the correlation among layer parameters for field data using GSA and PSO is either strongly positive or strongly negative, which describes that the parameters are dependent on each other. Thus a change in one parameter affects the other, and also apparent resistivity curve is very much involved.

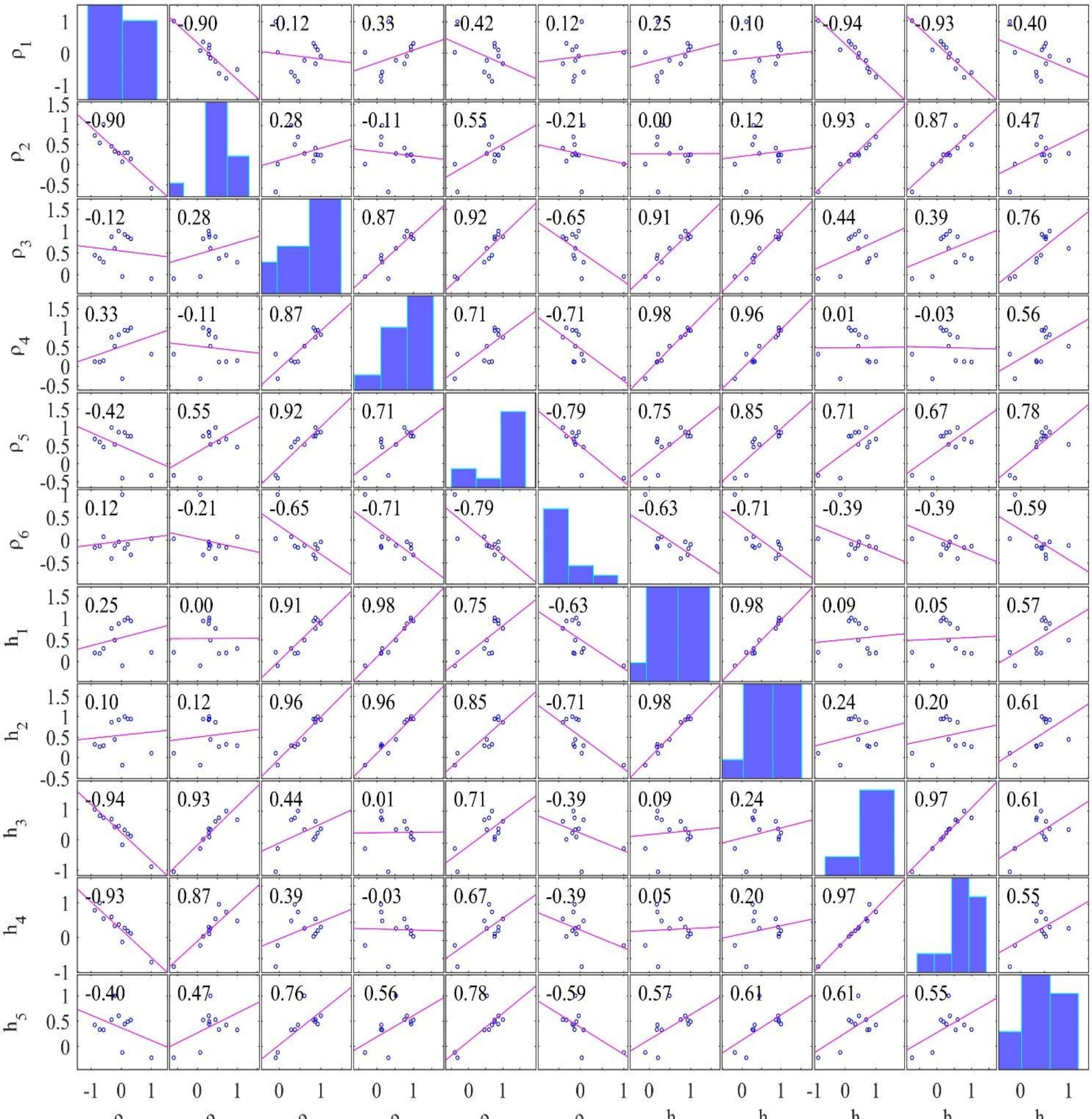

Figure 15 Correlation matrix of field data taken from the geothermal rich area, Island of Milos, Greece for PSO.

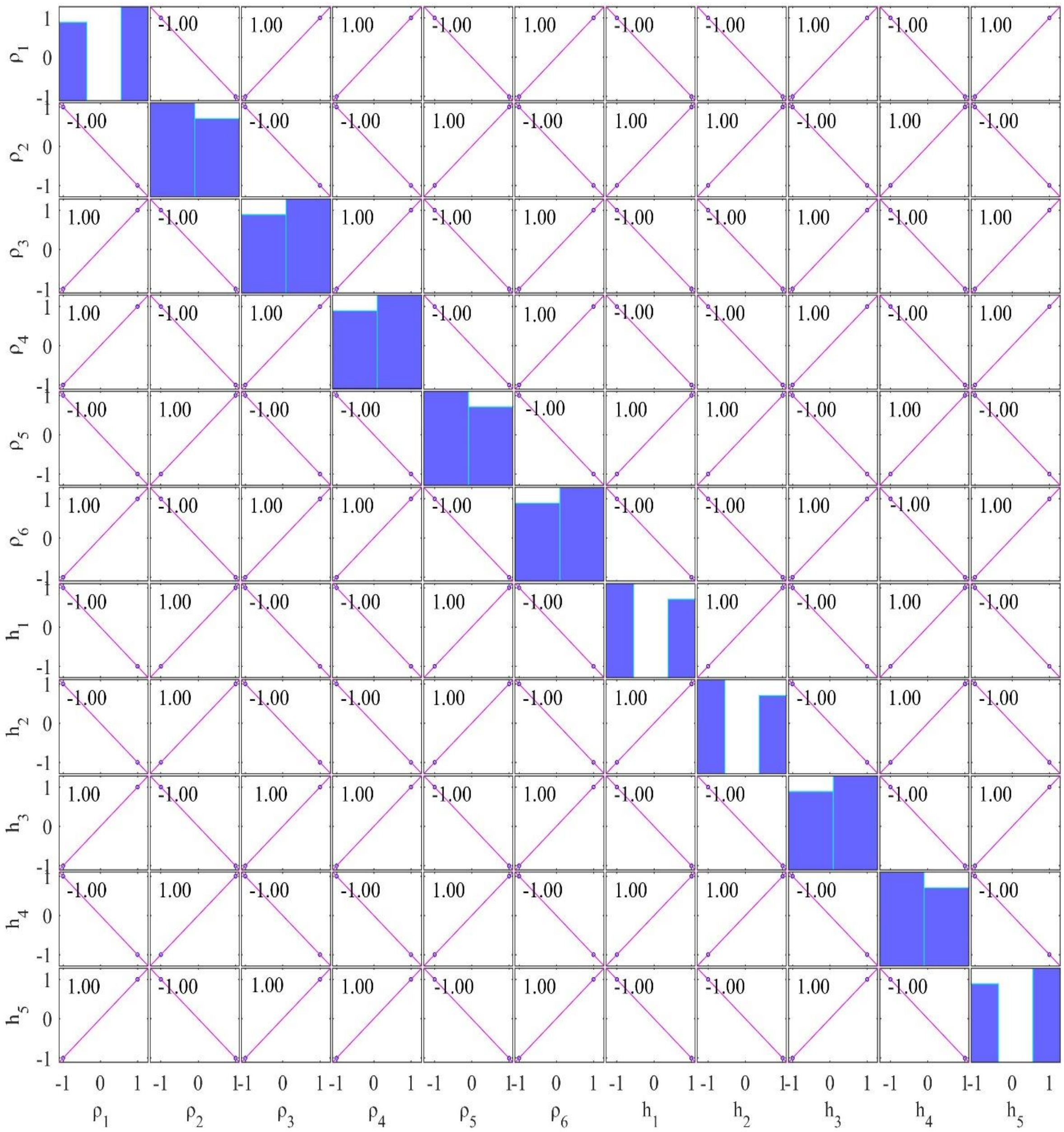

Figure 16 Correlation matrix of field data taken from island geothermal rich area of Milos, Greece for GSA.

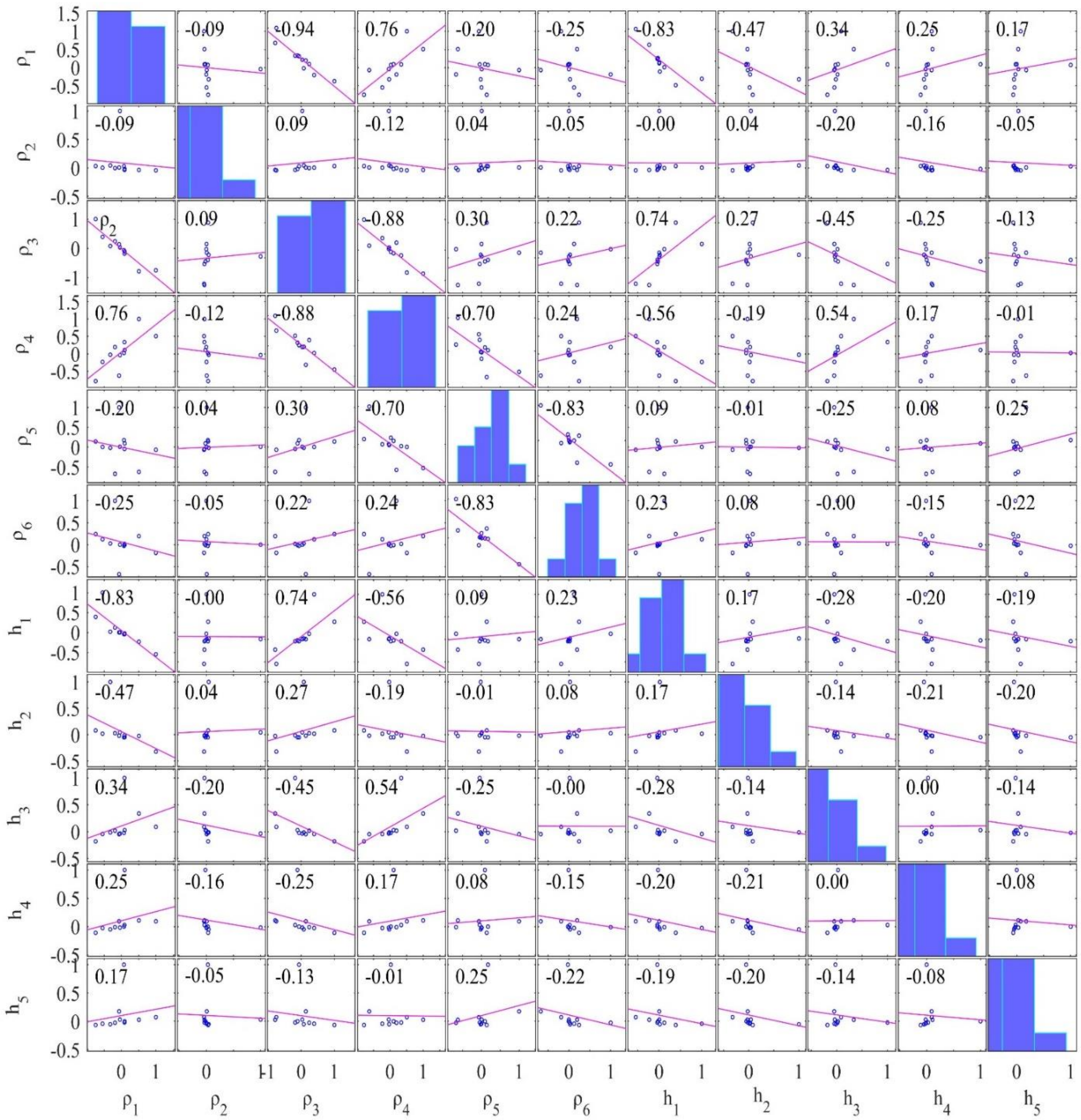

Figure 17 Correlation matrix of field data taken from island geothermal rich area of Milos, Greece for hybrid wPSOGSA.

3.4 Application to field MT data-Newcastleton, Southern upland, Scotland

Another field example of MT data was picked to illustrate our technique from Newcastleton (2.796° W, 55.196° N in Geographic coordinates), Southern Uplands of Scotland. The Southern Uplands are isolated from the Midland Valley by the Southern Uplands fault. The location of the MT site and the geology of the study area are shown in Fig. 18.

During nine days, in the frequency range of 0.1 Hz to 0.0001 Hz, the variations of the magnetic and telluric fields concerning the time at four sites along a line perpendicular to the anomaly's strike were recorded, keeping a high signal to noise ratio where the anisotropy ratios are so near to one and the skew factor is less than 0.1 for the majority of periods. Due to low anisotropy ratios and skew factor, the resistivity distribution under this location is one-dimensional (Jones and Hutton, 1979). Here one set of MT data is inverted using PSO, GSA, and wPSOGSA to obtain the best fitting apparent resistivity curve, apparent phase curve, and 1D depth model as shown in subfigures Fig. 19(a), Fig. 19(b), and Fig. 19(c), respectively. Figure 19 shows a realistic one-dimensional resistivity variation with a phase response ranging from 60° at 100 seconds to 35° at 1000 seconds, which can only be obtained by establishing a conducting zone at lower crustal/upper mantle levels (Jones and Hutton, 1979).

The execution time for wPSOGSA (33 seconds) is the least as compared to GSA (34 seconds) and PSO (53 seconds). The convergence iterations of PSO, GSA, and wPSOGSA are 79, 101, and 65, and its associated misfit errors are 3.79, 4.72, and 3.70, respectively.

The inverted MT model is illustrated in subfigure Fig. 19(c), which depicts two low conductive zones at a depth of 21 km and 400 km. The first conductive layer (70 Ωm) with a thickness of 28 km is underlain by a high resistive top layer of thickness of 21 km, and the second very high conductive layer (less than 1.0 Ωm) at a depth of 400 km is underlain by high resistive layer (550 Ωm) of thickness 351 km. Thus, the last layer of a very high conductive zone (i.e., resistivity less than 1.0 Ωm) as a lower crust/upper mantle conductor at a depth of 400 km is estimated. At 400 m depths, a conducting zone meets both the amplitude and phase long period responses. This explanation is directly equivalent to accepted models derived from Monte-Carlo models for the structure underlying the Southern Uplands.

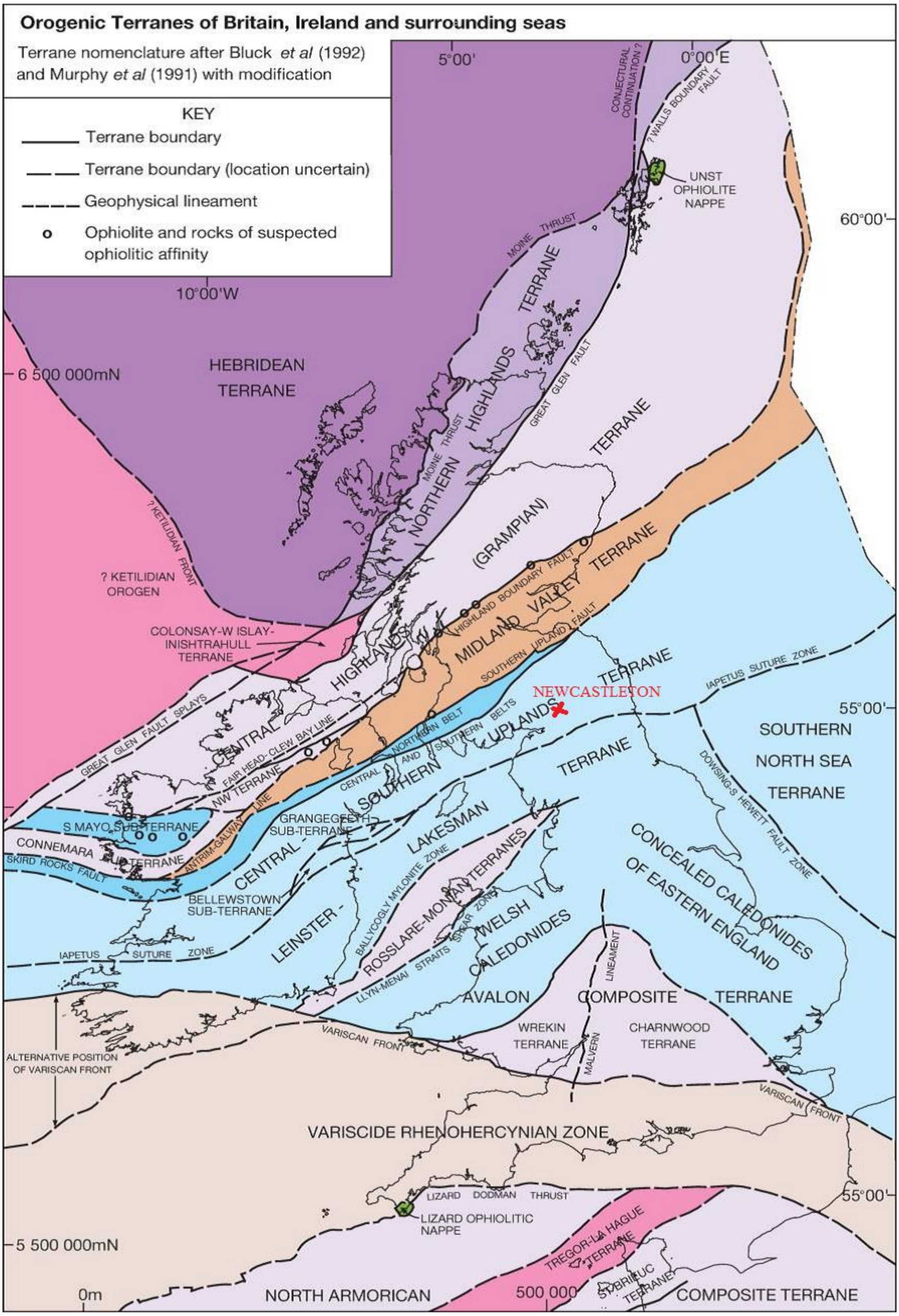

Figure 18 The location of MT site and geology of the Southern upland, Scotland (after BGS, 2016).

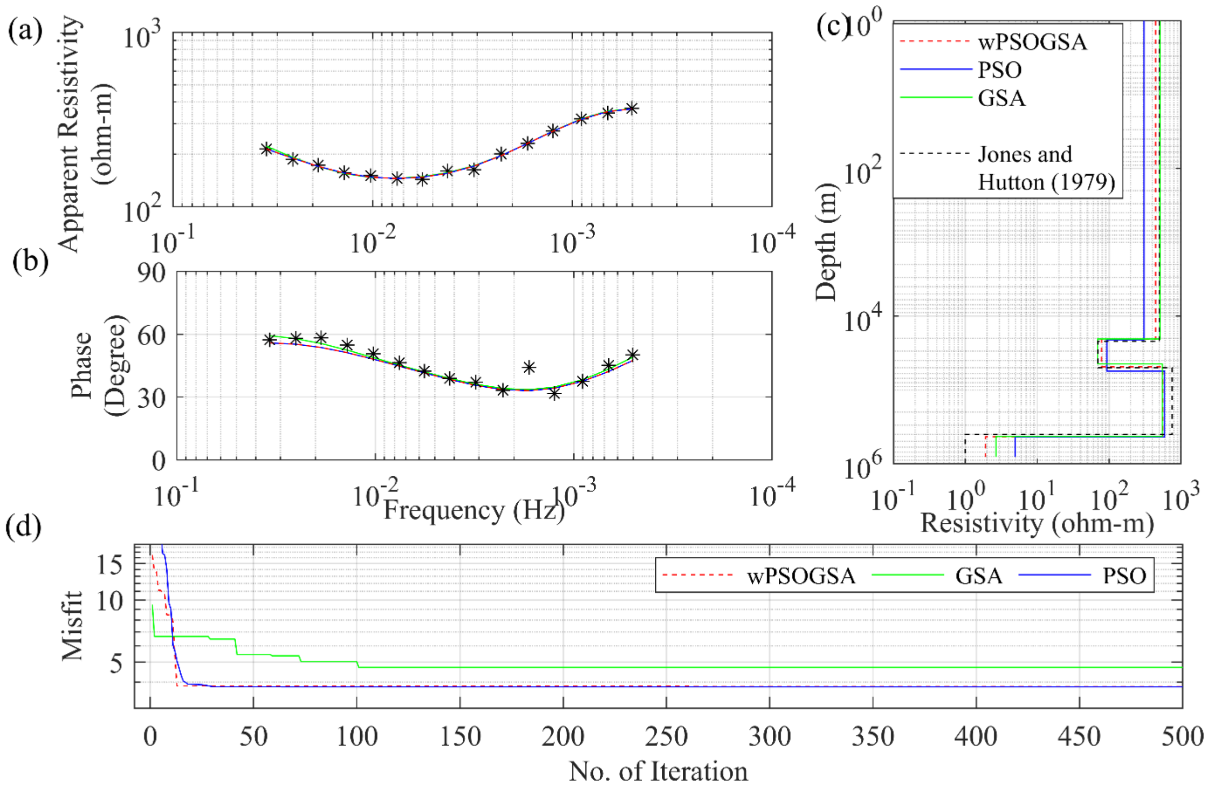

Figure 19 The inverted MT response by PSO (blue color), GSA (green color), and hybrid wPSOGSA (red color) with a true model (black color) over Newcastleton, Southern Scotland, as shown in (a) observed and calculated apparent resistivity curve, (b) observed and calculated apparent phase curve, (c) 1D depth inverted model and (d) convergence curve.

Table 6 Search range, inverted results by posterior PDF (68.27 % CI) using PSO, GSA, and wPSOGSA for field data.

Layer parameters		ρ_1 (Ωm)	ρ_2 (Ωm)	ρ_3 (Ωm)	ρ_4 (Ωm)	h_1 (m)	h_2 (m)	h_3 (m)
Search Range		300-1000	10-150	250-1500	0.1-5	10000-30000	15000-35000	100000-450000
Mean Posterior	PSO	304.47	92.66	591.52	4.93	20894.01	34776.15	379563.48
	GSA	507.65	69.38	548.46	2.66	20493.18	24182.99	382090.23
	wPSOGSA	444.27	78.94	554.53	1.91	20591.39	28177.40	382181.50
Jones and Hutton (1979a)	Monte-Carlo Inversion	500.00	70.00	750.00	1.00	22000.00	28000.00	350000.00

4.0 Discussions

The analysis on the two synthetic MT datasets shows that the proposed algorithm work very well and provide encouraging well fitted calculated apparent resistivity and phase data with the observed data. Also from the study, it is noted that the proposed algorithm is less sensitive to the search range and the constraints used in this algorithm. And the comparison of the model parameters show that the output from the proposed algorithm is very precise to the true model and faster than the individual algorithms and the other algorithms used in the previous papers.

Table 7 Inverted results by Dawes method, Jupp and Vozoff method, the Fischer inversion method (resistivity in Ωm) and Parker D+ Inversion.

Layer Parameters	The Dawes method - a hybrid Monte Carlo	The Jupp and Vozoff method	The Fischer inversion	Parker D+ Conduc-tance (Siemens)	Layer Parameters	The Dawes method - a hybrid Monte Carlo	The Jupp and Vozoff method	The Fischer inversion	Parker D+
ρ_1 (Ωm)	20.25875	14.600889	10.217801	46.00	h_1 (m)	12.98136	13.1712586	12.580575	34.00
ρ_2 (Ωm)	0.510194	0.51276562	0.5135027	65.00	h_2 (m)	136.2889	136.313007	21.962187	64.20
ρ_3 (Ωm)	3.663892	4.4639495	0.6283345	70.00	h_3 (m)	1298.206	1670.17267	103.19952	198.77
ρ_4 (Ωm)	35.83218	202.73303	3.7222432	172.00	h_4 (m)	12846.85	1705.7833	31.24917	737.04
ρ_5 (Ωm)	69.23081	28.907505	6.6645056	177.00	h_5 (m)	---	9777.8286	68.60352	1062.35
ρ_6 (Ωm)	---	93.942774	3.6770724		h_6 (m)	---	---	1485.8284	
ρ_7 (Ωm)	---	---	19.826915		h_7 (m)	---	---	5607.5719	
ρ_8 (Ωm)	---	---	33.372876			---	---	---	

A research conducted by Hutton et al. (1989), compare various techniques, including Parker H+, Dawes (a combined Monte Carlo/Hedgehog approach developed by Dawes), Jupp-Vozoff, Fischer, and Parker D+ inversions, to interpret the subsurface geology of the Island of Milos, Greece. Among these techniques, the Dawes algorithm proved to be the most effective in identifying a reservoir interface at the borehole's depth. Consequently, these methods were utilized to compile 1-D models along several traverses. All three models, Parker H+, Parker D+, and Dawes, indicate the presence of a resistivity boundary at a depth of approximately 1000 m (Hutton et al., 1989), where the geothermal reservoir has been detected. The research findings through proposed algorithm reveal that the resistivity of the crystalline basement beneath the geothermal site is abnormally low (< 20 Ωm) in the uppermost portion and remains below 50 Ωm at depths of at least 10 km.

The subfigure in Fig. 19(c) presents the inverted MT model of the Southern upland, Scotland, displaying two zones of low conductivity at depths of 21 km and 400 km. Contrary to the findings of Jain and Wilson (1967), there is a strong evidence suggesting that the conducting zone (70 Ωm) beneath the Southern Uplands exists at a depth exceeding 20 km. Furthermore, there is a second layer of extremely high conductivity (representing lower crust/upper mantle of less than 1.0 Ωm) at a depth of 400 km, which is underlain by a highly resistive layer (550 Ωm) spanning a thickness of 351 km. At a depth of 400 m, this conducting zone shows a direct alignment with both the amplitude and phase responses of long period measurements, which can be notice in the model derived from Monte-Carlo simulations of the structure underlying the Southern Uplands (see Fig. 19). The results from proposed algorithm as well as from PSO and GSA (see Fig. 19), demonstrate the presence of a highly conductive layer at depths exceeding 20 km and 400 km, corroborating with the findings of (Jones and Hutton, 1979).

5.0 Conclusions

The study presented the wPSOGSA algorithm along with PSO and GSA to evaluate their efficacy and applicability to the MT data, which narrates the appraisal of 1D resistivity models from apparent resistivity, apparent phase, and the frequency data sets. So, synthetic and field MT data from various geological terrains were used to demonstrate the relevance of these methods, which are further carried out by applying multiple runs, generating a large number of models that fit the apparent resistivity and apparent phase curves. Furthermore, these best-fitting models within a specified range are then chosen for statistical analysis. The statistical analysis includes posterior PDF based on the Bayesian approach with 68.27 % CI, correlation matrix, and stability analysis are used to understand the accuracy of the mean model and its uncertainty. However, the solution from the posterior PDF based on the Bayesian of wPSOGSA is better than GSA and PSO, explaining the reliability of the proposed inversion algorithm. In general, conventional techniques can effectively resolve the model in random noise, but they can miscarry in methodical error or inappropriate models, also, the performance of the proposed algorithms on field datasets has been analyzed based on the mean model, uncertainty, correlation and stability of layered earth models, and found that the results obtained from wPSOGSA are reliable, stable, and more accurate than the available results, that are well adapted to borehole lithology.

Acknowledgments

The authors would like to express their gratitude to the IIT(ISM), Dhanbad, for providing a pleasant environment to pursue this study and support for the research. We also express our gratitude to the Editor-in-Chief, Associate Editor, and anonymous reviewers, whose suggestions and comments enabled us to better understanding of the issue and considerably improve our manuscript.

Declarations

Competing interests

The authors have no relevant financial or non-financial interests to disclose and no competing interests to declare that are relevant to the content of this article. All authors certify that they have no affiliations with or involvement in any organization or entity with any financial interest or non-financial interest in the subject matter or materials discussed in this manuscript.

Data availability statement

The datasets used for the present study and analysis have been taken from published paper, cited in the manuscript.

Authors' contribution statement

Mukesh: Conceptualization of the study, Methodology, Computer code, Analysis, Drafting of the manuscript.

Kuldeep Sarkar: Methodology, Computer code, Analysis, Drafting the manuscript

Upendra K. Singh: Supervision, Suggestions, and editing.

References

Ai, H., Essa, K. S., Ekinci, Y. L., Balkaya, Ç., Li, H., and Géraud, Y.: Magnetic anomaly inversion through the novel barnacles mating optimization algorithm, Sci. Rep., 12, 22578, https://doi.org/10.1038/s41598-022-26265-0, 2022.

Cagniard, L.: Basic theory of the magneto-telluric method of geophysical prospecting, Geophys, 18, 605–635, https://doi.org/10.1190/1.1437915, 1953.

Colorni, A., Dorigo, M., and Maniezzo, V.: Distributed Optimization by Ant Colonies, Proceedings of the First European Conference on Artificial Life, Paris, France, 134–142 pp., 1991.

Constable, S. C., Parker, R. L., and Constable, C. G.: Occam's inversion: A practical algorithm for generating smooth models from electromagnetic sounding data, Geophys, 52, 289–300, https://doi.org/10.1190/1.1442303, 1987.

"Dawes, G. J. K. ": Magnetotelluric feasibility study: Island of Milos, Greece, Luxembourg, 1986.

Dosso, S. E. and Oldenburg, D. W.: Magnetotelluric appraisal using simulated annealing, Geophys. J. Int., 106, 379–385, https://doi.org/10.1111/j.1365-246X.1991.tb03899.x, 1991.

Essa, K. S. and Diab, Z. E.: Gravity data inversion applying a metaheuristic Bat algorithm for various ore and mineral models, J. Geodyn., 155, 101953, https://doi.org/10.1016/j.jog.2022.101953, 2023.

Essa, K. S., Abo-Ezz, E. R., Géraud, Y., and Diraison, M.: A successful inversion of magnetic anomalies related to 2D dyke-models by a particle swarm scheme, J. Earth Syst. Sci., 132, 65, https://doi.org/10.1007/s12040-023-02075-4, 2023.

Hutton, V. R. S., Galanopoulos, D., Dawes, G. J. K., and Pickup, G. E.: A high resolution magnetotelluric survey of the Milos geothermal prospect, Geothermics, 18, 521–532, https://doi.org/10.1016/0375-6505(89)90054-0, 1989.

Jain, S. and Wilson, C. D. V.: Magneto-Telluric Investigations in the Irish Sea and Southern Scotland, Geophys. J. Int., 12, 165–180, https://doi.org/10.1111/j.1365-246X.1967.tb03113.x, 1967.

Jones, A. G. and Hutton, R.: A multi-station magnetotelluric study in southern Scotland – I. Fieldwork, data analysis and results, Geophys. J. Int., 56, 329–349, https://doi.org/10.1111/j.1365-246X.1979.tb00168.x, 1979.

Kennedy, J. and Eberhart, R.: Particle swarm optimization, in: Proceedings of ICNN'95 - International Conference on Neural Networks, 1942–1948 vol.4, https://doi.org/10.1109/ICNN.1995.488968, 1995.

Khishe, M. and Mosavi, M. R.: Chimp optimization algorithm, Expert Syst. Appl., 149, 113338, https://doi.org/10.1016/j.eswa.2020.113338, 2020.

Kirkpatrick, S., Gelatt C., D., and Vecchi M., P.: Optimization by Simulated Annealing, Science, 220, 671–680, https://doi.org/10.1126/science.220.4598.671, 1983.

Kunche, P., Sasi Bhushan Rao, G., Reddy, K. V. V. S., and Uma Maheswari, R.: A new approach to dual channel speech enhancement based on hybrid PSOGSA, Int. J. Speech Technol., 18, 45–56, https://doi.org/10.1007/s10772-014-9245-5, 2015.

Li, S.-Y., Wang, S.-M., Wang, P.-F., Su, X.-L., Zhang, X.-S., and Dong, Z.-H.: An improved grey wolf optimizer algorithm for the inversion of geoelectrical data, Acta Geophys., 66, 607–621, https://doi.org/10.1007/s11600-018-0148-8, 2018.

Lynch, S. M.: Introduction to applied Bayesian statistics and estimation for social scientists, Springer, New York, 2007.

Miecznik, J., Wojdyła, M., and Danek, T.: Application of nonlinear methods to inversion of 1D magnetotelluric sounding data based on very fast simulated annealing, Acta Geophys. Pol., Vol. 51, nr 3, 307–322, 2003.

Mirjalili, S. and Hashim, S. Z. M.: A new hybrid PSOGSA algorithm for function optimization, in: 2010 International Conference on Computer and Information Application, 374–377, https://doi.org/10.1109/ICCIA.2010.6141614, 2010.

Mirjalili, S., Mirjalili, S. M., and Lewis, A.: Grey Wolf Optimizer, Adv. Eng. Softw., 69, 46–61, https://doi.org/10.1016/j.advengsoft.2013.12.007, 2014.

Nabighian, M. N. and Asten, M. W.: Metalliferous mining geophysics—State of the art in the last decade of the 20th century and the beginning of the new millennium, Geophysics, 67, 964–978, https://doi.org/10.1190/1.1484538, 2002.

Pace, F., Raftogianni, A., and Godio, A.: A Comparative Analysis of Three Computational-Intelligence Metaheuristic Methods for the Optimization of TDEM Data, Pure Appl. Geophys., 179, 3727–3749, https://doi.org/10.1007/s00024-022-03166-x, 2022.

Pérez-Flores, M. A. and Schultz, A.: Application of 2-D inversion with genetic algorithms to magnetotelluric data from geothermal areas, Earth Planets Space, 54, 607–616, https://doi.org/10.1186/BF03353049, 2002.

Rashedi, E., Nezamabadi-pour, H., and Saryazdi, S.: GSA: A Gravitational Search Algorithm, Inf. Sci., 179, 2232–2248, https://doi.org/10.1016/j.ins.2009.03.004, 2009.

Rodi, W. and Mackie, R. L.: Nonlinear conjugate gradients algorithm for 2-D magnetotelluric inversion, Geophysics, 66, 174–187, https://doi.org/10.1190/1.1444893, 2001.

Ross, S.: Probability and statistics for engineers and scientists, Elsevier, New Delhi, 2009.

Roy, A. and Kumar, T. S.: Gravity inversion of 2D fault having variable density contrast using particle swarm optimization, Geophys. Prospect., 69, 1358–1374, https://doi.org/10.1111/1365-2478.13094, 2021.

Sen, M. K. and Stoffa, P. L.: Bayesian inference, Gibbs' sampler and uncertainty estimation in geophysical inversion1, Geophys. Prospect., 44, 313–350, https://doi.org/10.1111/j.1365-2478.1996.tb00152.x, 1996.

Sen, M. K. and Stoffa, P. L.: Global Optimization Methods in Geophysical Inversion, Cambridge University Press, Cambridge, https://doi.org/10.1017/CBO9780511997570, 2013.

Şenel, F. A., Gökçe, F., Yüksel, A. S., and Yiğit, T.: A novel hybrid PSO–GWO algorithm for optimization problems, Eng. Comput., 35, 1359–1373, https://doi.org/10.1007/s00366-018-0668-5, 2019.

Sharma, S. P.: VFSARES—a very fast simulated annealing FORTRAN program for interpretation of 1-D DC resistivity sounding data from various electrode arrays, Comput. Geosci., 42, 177–188, https://doi.org/10.1016/j.cageo.2011.08.029, 2012.

Shaw, R. and Srivastava, S.: Particle Swarm Optimization: A new tool to invert geophysical data, Geophysics, 72, https://doi.org/10.1190/1.2432481, 2007.

Simon, D.: Biogeography-Based Optimization, IEEE Trans. Evol. Comput., 12, 702–713, https://doi.org/10.1109/TEVC.2008.919004, 2008.

Simpson, F. and Bahr, K.: Practical Magnetotellurics, Cambridge University Press, 2005.

Stewart, A. L. and McPhie, J.: Facies architecture and Late Pliocene – Pleistocene evolution of a felsic volcanic island, Milos, Greece, Bull. Volcanol., 68, 703–726, https://doi.org/10.1007/s00445-005-0045-2, 2006.

Storn, R. and Price, K.: Differential Evolution – A Simple and Efficient Heuristic for global Optimization over Continuous Spaces, J. Glob. Optim., 11, 341–359, https://doi.org/10.1023/A:1008202821328, 1997.

Tarantola, A.: Inverse Problem Theory and Methods for Model Parameter Estimation, https://doi.org/10.1137/1.9780898717921, 2005.

Tarantola, A. and Valette, B.: Generalized nonlinear inverse problems solved using the least squares criterion, Rev. Geophys., 20, 219–232, https://doi.org/10.1029/RG020i002p00219, 1982.

Ward, S. H. and Hohmann, G. W.: 4. Electromagnetic Theory for Geophysical Applications, in: Electromagnetic Methods in Applied Geophysics: Volume 1, Theory, Society of Exploration Geophysicists, 130–311, https://doi.org/10.1190/1.9781560802631.ch4, 1988.

Wen, L., Cheng, J., Li, F., Zhao, J., Shi, Z., and Zhang, H.: Global optimization of controlled source audio-frequency magnetotelluric data with an improved artificial bee colony algorithm, J. Appl. Geophys., 170, 103845, https://doi.org/10.1016/j.jappgeo.2019.103845, 2019.

Whitley, D.: A genetic algorithm tutorial, Stat. Comput., 4, 65–85, https://doi.org/10.1007/BF00175354, 1994.

Xiong, J., Liu, C., Chen, Y., and Zhang, S.: A non-linear geophysical inversion algorithm for the mt data based on improved differential evolution, Eng. Lett., 26, 161–170, 2018.

Yang, X.-S.: A New Metaheuristic Bat-Inspired Algorithm, in: Nature Inspired Cooperative Strategies for Optimization (NICSO 2010), edited by: González, J. R., Pelta, D. A., Cruz, C., Terrazas, G., and Krasnogor, N., Springer Berlin Heidelberg, Berlin, Heidelberg, 65–74, https://doi.org/10.1007/978-3-642-12538-6_6, 2010a.

Yang, X.-S.: Firefly algorithm, stochastic test functions and design optimisation, Int J Bio Inspired Comput, 2, 78–84, https://doi.org/10.48550/arxiv.1003.1409, 2010b.

Zhang, Z., Ding, S., and Jia, W.: A hybrid optimization algorithm based on cuckoo search and differential evolution for solving constrained engineering problems, Eng. Appl. Artif. Intell., 85, 254–268, https://doi.org/10.1016/j.engappai.2019.06.017, 2019.